ELSEVIER

Journal of Nuclear Materials 244 (1997) 227–250

journal of nuclear materials

Amorphization of intermetallic compounds under irradiation – A review

Arthur T. Motta *

Department of Nuclear Engineering, 231 Sackett Building, The Pennsylvania State University, University Park, PA 16802, USA

Received 21 March 1996; accepted 22 November 1996

Abstract

This is a review of the field of irradiation-induced amorphization of intermetallic compounds. It includes an update of recent experimental results using in-situ particle irradiation showing the effects of dose rate, temperature, crystal orientation, electron energy and the presence of stacking faults. The review describes amorphization by ion, electron and neutron irradiation in the context of a kinetic description, where the rate-limiting step is the accumulation of enough radiation damage in the lattice opposed by thermal annealing. Stability criteria, thermodynamic or otherwise, are combined with kinetics of radiation damage and annealing to provide an overall description of the amorphization process, and of the experimentally measured critical dose and critical temperature of amorphization. From the experimental observations, it is proposed that irradiation-induced amorphization in intermetallic compounds is an entropy-driven transformation, caused by the need of the material to maintain short-range order while accommodating the random ballistic motions of the atoms caused by irradiation.

1. Introduction

In recent years, many studies have considered the formation of amorphous phases in intermetallic compounds when submitted to irradiation, a process called irradiation-induced amorphization. The formation of amorphous phases in ceramics and minerals is well documented: the recognition of 'metamict' phases as being amorphous from self-irradiation dates back to 1893 [1]. Semiconductors such as Si and Ge are also susceptible to amorphization under irradiation [2]. The discovery that intermetallic compounds can be made amorphous by irradiation sparked great interest, as it was previously thought that the absence of charge localization and directional restrictions on bonding (present in ceramics and semiconductors) precluded irradiation-induced amorphization in intermetallic compounds. This raised the question of how enough energy to drive the transformation is stored in the lattice of intermetallic compounds, since damage annealing should be easier in the absence of bonding and charge restrictions.

Recently published reviews of this field [3–11] show that a large number of intermetallic compounds undergo amorphization under a variety of conditions. Amorphization occurs under neutron, ion and electron irradiation, in a wide range of temperatures. No pure metals (with the possible exception of Bi and Ga), or stable metallic solid solutions become amorphous under particle irradiation which points to the crucial role of chemical disordering in promoting amorphization under irradiation. Several empirical correlations for amorphization have been developed [12–15] and comprehensive theories put forth to rationalize amorphization [8,10,16]. These theories and empirical correlations attempt to predict which compounds undergo amorphization, or to derive conditions for amorphization to occur.

In amorphization of crystalline intermetallic compounds under irradiation a thermodynamically unfavored phase (the amorphous phase) replaces the thermodynamically stable crystal. Clearly, the kinetic restrictions imposed on the crystal by the influx of irradiating particles create the conditions for the amorphous phase to appear. Hence, to understand the amorphization process, it is necessary to understand the kinetics of radiation damage

* Fax: +1-814 862 8499.

PII S0022-3115(96)00740-4

and annealing in intermetallic compounds. This review presents the available kinetic data and uses it to construct a picture of amorphization that is closely related to the quantities measured experimentally, and that takes full account of the influence of different particles, dose rate and temperature. After a brief review of amorphization in non-metallic systems and of amorphization by means other than irradiation, the experimental evidence gathered on the amorphization of intermetallic compounds by particle irradiation is reviewed in Section 2. The theoretical understanding of irradiation-induced amorphization developed over the last decade is discussed in Sections 3.1 and 3.2. In the last part of Section 3 a new model to understand amorphization is proposed based on the increased entropy of the amorphous state compared with that of the defected crystal.

2. Radiation-induced amorphization: Experiments

The crystalline-to-amorphous transformation (amorphization) refers to the complete loss of long-range crystallographic order, as measured by X-ray diffraction or electron diffraction. Upon amorphization, the sharp lines from X-ray patterns are replaced by a liquid-like distribution function associated with amorphous materials. In the case of electron diffraction, the crystalline spot pattern is replaced by an amorphous halo. Amorphization can be detected by a variety of techniques, including the isotropy of material properties [2], changes in electrical resistivity [17–19], specific heat [20], Rutherford backscattering (RBS) [19,21,20], neutron reflectivity [22], Mössbauer spectroscopy [21], electron energy loss spectroscopy [23], fractography [24], and Raman spectroscopy [25]. Diffraction gives direct information on the structural changes accompanying amorphization and is the main detection method considered in this review.

2.1. Amorphization in non-metallic systems

Amorphization by particle irradiation is well known in non-metallic compounds, such as ceramics, semiconductors and ionic compounds. These are briefly reviewed in the following.

Ceramics and minerals: The amorphization of ceramics and minerals under charged-particle irradiation has been reviewed before [26]. Survey-type experiments have been conducted to determine amorphization susceptibility [27], and empirical criteria have been developed to predict amorphization behavior [28]. The study of irradiation-induced amorphization in minerals such as zircon has been particularly fruitful because of the wide range of dose rates available: in geologic deposits amorphization from self-irradiation has a dose rate of 10^{-16} displacements per atom (dpa) s^{-1} [29,30], while amorphization by particle irradiation can have dose rates up to 10^{-2} and 10^{-3} dpa s^{-1} [31]. Many of the features seen in the amorphization of ceramics are also seen in the amorphization of intermetallic compounds: large differences in displacement energies among the individual sublattices [32,33], large differences in critical temperature between ion and electron-induced amorphization [34], influence of dose rate [29,35], and 'stages' in the dose-to-amorphization at temperatures below the critical temperature for amorphization [31]. Finally, the amorphization mechanism in ceramics can also be regarded as a loss of topological long-range order (LRO) while maintaining short-range order (SRO) [36].

Several ceramics of technological interest have been studied to somewhat greater extent. A recent study finds that MgO (magnesia), $MgAl_2O_4$ (spinel) and Al_2O_3 (alumina) do not amorphize after room temperature ion irradiation, except when irradiated by certain types of ions (I in spinel, Zr in alumina and Ti in magnesia) [37]. Other studies have shown amorphization in spinel by Ar ion irradiation below 100 K [38]. The presence of equivalent cation sites in spinel has been linked to its irradiation behavior [39].

The amorphization of quartz has also been extensively studied [40]. Quartz, as well as other minerals, undergoes amorphization by pressure [25,41], as well as being amorphized by irradiation, including high energy ions [42]. Pressure-induced amorphization has been observed for only a few metallic systems [43]. Another compound that has received detailed attention is SiC [44]. The temperature dependence of the dose-to-amorphization has been determined for SiC under Xe ion irradiation and it is found that there is a difference of approximately 200 K between the critical temperature for Xe ion irradiation (500 K) and for electron irradiation (300 K) [45,46]. Detailed high resolution electron microscopy studies of amorphization in ceramics have been attempted [45,47], but have generally been limited to describing amorphization in qualitative terms [40]. Similar studies have been conducted for intermetallic compounds [48,49].

Similarly to intermetallic compounds, the crystal structure of ceramics can be described as an ordered arrangement of polyhedra [50]. In his topology-based model of irradiation-induced amorphization of ceramics, Hobbs [40,51] emphasize the role of alterations in short-range correlations that cannot be accommodated in a solid whose long-range order does not allow much structural freedom. The lack of structural freedom can be deduced from the topological properties of the structure, especially the connectivity of the composing polytopes.

Semiconductors: The amorphization of Si by particle bombardment has important technological implications, and because of this has been extensively studied [52]. In particular, the problem of finding the rate of advancement of an amorphous layer into a crystalline layer (or of the crystalline into the amorphous) in Si and Ge in particular has received great attention [53,54]. As the irradiation tempera-

ture increases, the amorphization rate decreases until it stops at the critical temperature. Another interesting feature is that approximately 10 K above the critical temperature the process is reversed and the crystalline layer starts to advance at the expense of the amorphous layer. A recent model proposed by Carter [55] further refines these concepts and proposes a mechanistic understanding of amorphization in ion-implanted semiconductors, considering the effects of flux and temperature. Si has also been used to demonstrate that concurrent electron and ion irradiation increase the dose-to-amorphization compared to ion irradiation, possibly due to the higher percentage of isolated point defects created by electron irradiation which promote radiation damage annealing [56,57]. One interesting aspect of amorphization of Si by particle irradiation is that it is not possible to amorphize Si by electron irradiation, even at very low temperatures [58]. In fact, electron irradiation hinders, rather than helps, amorphization upon dual electron and ion irradiation of Si [58].

The presence of structural disorder and amorphization of carbon compounds has been reviewed in [59]. In graphite, amorphization has been produced by electron and ion irradiation [60] and neutron irradiation [61]. The critical temperature for amorphization under electron irradiation is 580 K [36]. The authors note that the large distance between basal planes reduces the effects of cascades (the difference between the dose-to-amorphization at room temperature by different ions is small). Finally a particular type of ceramic where irradiation-induced amorphization has received great attention lately are the Y–Ba–Cu–O high temperature superconducting compounds [62], where a dose rate effect is also found [63].

2.2. Amorphization in intermetallic compounds

Amorphization in metallic systems (intermetallic compounds, metallic multilayers, metallic solid solutions) has been produced by different means such as solid-state reaction [9], pressure [25,43], ball milling [64–66], cold plastic deformation [67], hydrogenation [68–70], and irradiation [4,6,71]. The case of hydrogenation is somewhat different from the others in that the composition is not held constant during the experiment. The preferred formation of metal–H bonds over metal–metal bonds could then be a driving force for the loss of long-range order [69,70]. The influence of alloying elements, either present in the alloy [72] or introduced by irradiation [73] creates an additional chemical driving force for amorphization in the affected compounds. The common ground of amorphization by solid state reaction, ball milling and irradiation, is that in each case either the appearance or the permanence of the more energetically favorable intermetallic phase is precluded by kinetic constraints. The difference is that amorphization by solid-state reaction occurs in the direction of decreasing system free energy while with irradiation and ball-milling it is the reverse.

In the case of amorphization by *solid-state reaction* in metallic multilayers of elements with large negative heat of mixing, the appearance of the amorphous phase represents a *decrease* in the total system energy compared to the unreacted state. Fig. 1 shows the free energy of two metals with negative heat of mixing (Zr and Fe), both for an amorphous phase (ΔG_A) and for a crystalline solid solution of atoms (ΔG_S) [74]. The dotted line indicates the free energy of a mechanical mixture of Zr and Fe. There is a large energy gain from forming an amorphous phase as compared to the mechanical mixture. The free energy difference between the amorphous phase and the intermetallic compound is comparatively small. A negative heat of mixing is however, not a necessary condition for amorphization as the existence of amorphization in systems with positive heats of mixing has recently elicited great interest [75,76]. Solid state thermal reaction in metallic multilayers produces either one of the stable intermetallic compounds or the amorphous phase depending on the relative diffusivities of the elements, on the multilayer composition and wavelength, and interface reaction rates, as described by Gösele and Tu [77]. Amorphization by irradiation of metallic multilayers is subject to the driving forces present in the purely thermal case, in addition to irradiation mixing and disordering, which decreases the time to amorphization and expands the region where amorphization is possible [78]. Irradiation has two main effects: the creation of a supersaturation of defects that can accelerate thermal processes and ballistic mixing and disordering [79], which tends to take the material away from equilibrium [80].

In the case of *irradiation and ball milling*, the amorphous phase is arrived at via a different route: the stable intermetallic phase is present at the outset, but is destabilized by various mechanisms of damage accumulation, allowing the amorphous phase to appear. A net energy *increase* occurs in this case. Most of this paper is devoted

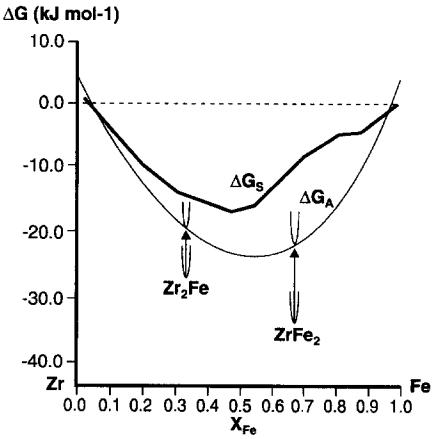

Fig. 1. Free energy versus concentration for the phases in the Zr–Fe system (from Ref. [74]).

to understanding the driving forces and the kinetics of the process of irradiation-induced amorphization.

2.3. Amorphization under different types of irradiation: General remarks

Amorphization of intermetallic compounds has been observed under both neutron and charged-particle irradiation, although because of the obvious difficulties in irradiating with neutrons those observations have been considerably less frequent [4]. In general, charged-particle irradiation has proven to be a flexible and powerful tool for studying amorphization [8]. Experiments can be done 'in-situ' in high voltage electron microscopes so that the transformation morphology and kinetics can be directly determined. In some facilities, such as the IVEM (intermediate voltage electron microscope) at Argonne National Laboratory, it is possible to irradiate the sample with ions in the microscope while observing with electrons. It is possible to vary irradiation conditions, such as temperature and dose rate in a wide range. In addition, the displacement rates in accelerators are orders of magnitude higher than those in reactors allowing the damage in displacements per atom equivalent to years in a reactor to be reached within hours or minutes.

There are two main distinctions between different types of irradiation. The first is between cascade-producing irradiation (ion and neutron) and irradiation that produces isolated Frenkel pairs (gamma and electron irradiation). The high density of energy deposition in collision cascades can raise local damage levels to very high values, which are correspondingly more difficult to anneal. This is likely why the critical temperature for amorphization under cascade-producing irradiation is higher than under electron radiation [81,82] and why some compounds amorphize under ion irradiation but not under electron irradiation [83–86]. The second distinction is between neutron and charged-particle irradiation. Since the overall displacement rate in neutron irradiation is much lower than in charged particle irradiation, processes depending on thermal diffusion, such as damage annealing, are favored under neutron irradiation when compared to charged particle irradiation.

Bellon and Martin [87] have identified the parameter γ (ratio of collisional displacements to thermal jumps) as an important factor in predicting the behavior of a material under irradiation. Table 1 shows that, because of the different displacement rates, for a given irradiation temperature and a given dose γ is different for each of the different irradiation conditions. Although mild from the point of view of damage localization, electron irradiation is a much more efficient way of producing freely-migrating defects than cascade producing irradiation, since essentially all the defects produced can undergo long-range diffusion, while a large fraction of the ion and neutron produced defects are annealed out during cascade cooling [88].

Differences in beam orientation (isotropic for neutrons, directional for charged-particles), specimen geometry, size of irradiated region, energy distribution of irradiation, also have to be taken into account. A summary of the differences between the irradiations is shown in Table 1, for conditions found in typical irradiation facilities. For example, although the practical overall displacement rates for electron irradiation are considerably higher than for neutron and ion irradiation, the presence of cascades in the latter raises the local displacement rates to much higher levels, so that electron irradiation can be considered a milder form of irradiation, and the damage it produces can therefore be annealed at a lower temperature. Another factor that needs to be considered is the proximity of free surfaces in charged particle irradiation which provides a strong defect sink not present under neutron irradiation [89].

Thus, changing the irradiation conditions yields experimental information that cannot be directly compared. However, using these different types of irradiations coupled with appropriate theoretical modeling and computer simulation, it is possible to gain greater insight into the

Table 1
Correlation of neutron and charged-particle irradiation

	Neutron	Ion (heavy/light)	Electron
Typical flux (part./m^2s)	5×10^{17} (isotropic)	10^{15}–10^{16} (directional)	5×10^{23} (directional)
Displacement rate (dpa/s)	10^{-7}	10^{-4}–10^{-5}	10^{-2}–10^{-3}
Irradiation time (1 dpa)	~ 4 months	~ 1–24 h	2–20 m
Temperature	reactor (570 K)	adjustable	adjustable
Displacement profile	no	sharp peak @ end of range	no (if thin foil)
Sample geometry	bulk sample	semi-bulk (near surface)	thin foil (~ 100 nm)
Spatial distribution of damage	inhomogeneous (dense cascades)	inhomogeneous (variable cascade density)	homogeneous (Frenkel pairs only)
Free defect fraction	few %	~ 5–50%	~ 100%
Penetration depth (typical)	whole	1–10 μm	100 nm
Size of irrad. region	whole	~ 1 cm^2	~ 1 μm^2
In-situ exam.	no	usually no	yes

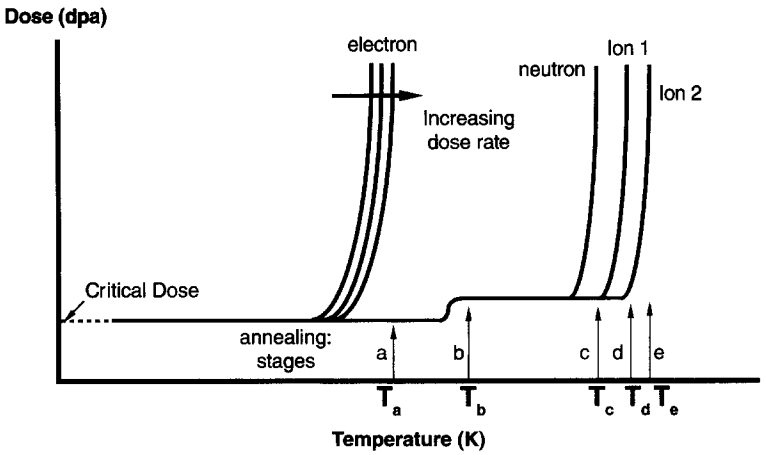

Fig. 2. Schematic dose-to-amorphization versus temperature for different types of irradiation.

physical processes at hand. No meaningful analysis of irradiation-induced amorphization, or any type of irradiation effect, can be done without a clear understanding of the different characteristics of the damage produced by the different irradiations. If that understanding is present and is incorporated into the theoretical model along with the detailed defect information from computer simulations, it is possible to produce a more detailed and broadly based mechanistic understanding of the kinetics of irradiation-induced amorphization in intermetallic compounds.

2.4. Dose-to-amorphization and critical temperature

Fig. 2 is a schematic representation of the dose-to-amorphization as a function of temperature for different types of irradiation. Several quantities measured from Fig. 2 have to be rationalized by any theoretical model. At low temperature, the dose-to-amorphization is independent of temperature. This dose is the *critical dose*-to-amorphization and represents a measure of the ability of the material to repair itself in the absence of thermal annealing. The irradiation damage accumulation kinetics have to be consistent with the value of the athermal dose. As the temperature increases the dose-to-amorphization rises. For electron irradiation above temperature T_a (with slight variations depending on dose rate), amorphization is not possible, so the temperature T_a is the *critical temperature for amorphization* under electron irradiation. Typically, amorphization by cascade-producing irradiation (ion and neutron irradiation) remains possible above T_a. At temperature T_b there is an increase in the dose-to-amorphization, from the athermal dose. This increase can be attributed to an annealing process that makes the damage accumulation process more difficult without completely impeding it, so an *annealing stage* occurs at temperature T_b. Other types of irradiation damage are successively overwhelmed at temperatures T_c, T_d and T_e which are, for example, the *critical temperatures* for neutron, ion type 1 and ion type 2, respectively. Ion type 2 is typically heavier than type 1. Theoretically, each type of ion has a slightly different critical temperature, depending on its damage structure, as discussed in Section 2.6.

One example of this type of curve is shown in Fig. 3 [90], obtained during amorphization of Zr_3Fe under Ar ion and electron irradiation. At low temperatures, the curves all coincide. At approximately 220 K, the dose-to-amorphization increases abruptly (at lower dose rates, the abrupt increase occurs at a slightly lower temperature). This is the critical temperature for amorphization in Zr_3Fe under electron irradiation. The increase in dose-to-amorphization under Ar ion irradiation is probably due to

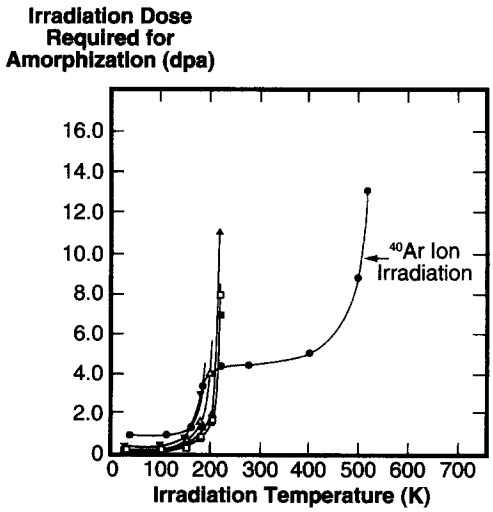

Fig. 3. Dose-to-amorphization in displacements per atom at various irradiation temperatures for 0.9 MeV electron and 0.5–1.5 MeV ^{40}Ar ion (●) irradiations of Zr_3Fe. Electron dose rate: ■, 1.83×10^{-3} dpa s^{-1}; □, 1.68×10^{-3} dpa s^{-1}; ▲, 1.47×10^{-3} dpa s^{-1}; △, 1.23×10^{-3} dpa s^{-1}; ▼, 1.04×10^{-3} dpa s^{-1}.

the increased annealing caused by the motion of a defect activated at that temperature. This defect increases the dose-to-amorphization by a factor of 4, but does not prevent it. Amorphization with Ar ions remains possible until 560 K, which is the critical temperature for Ar ion amorphization of Zr_3Fe. For Bi ions, (not shown) the critical temperature is somewhat higher, and the magnitude of the step at 220 K is smaller.

2.5. Amorphization kinetics

2.5.1. Measurement of dose rate

A typical amorphization sequence, obtained during amorphization of Zr_3Fe by electron irradiation at 200 K, is shown in Fig. 4. The beam is condensed to a 0.5 μm spot, and kept in place using fiducial marks in the sample. Amorphization is detected by the disappearance of the bend contours and in diffraction mode by the substitution of the spot pattern by a halo pattern characteristic of the amorphous phase. As explained below, the dose rate decreases with the distance from the center of the beam so that towards the edge, the dose rate is lower than at the center. In this particular case, after a long irradiation the radius of amorphous region saturates at a diameter smaller than the size of the beam (shown in Fig. 4F), indicating a dose rate effect.

The amorphization sequence in Fig. 4 suggests a way of obtaining the variation of the dose-to-amorphization with temperature and dose rate applicable to electron irradiation, which is shown in Fig. 5. The ratio of the amorphous region radius to the beam radius is measured as a function of dose for several temperatures, T_1 through T_5. The crystal-amorphous boundary is reasonably sharp as shown in Fig. 4, allowing a precise determination of the amorphous radius, using both the interruption of bend contours and the insensitivity of the bright field image of the irradiated region to tilt as criteria for amorphization. Low order bend contours are usually chosen to monitor amorphization (since they are the last to disappear before amorphization). A typical error bar in the measurement of the amorphous radius is also shown in Fig. 5.

The dose rate at different radial locations varies because of the Gaussian profile of the beam intensity. By performing careful electron dosimetry, it is possible to correlate the radial distance from the center of the beam spot with a given dose rate, as explained in [91], and illustrated in the upper part of Fig. 5. The dose is measured by two Faraday cups, one that captures the integrated intensity of the whole beam and another that captures the peak density. The two measurements completely determine the Gaussian profile of the electron beam. Several checks of this dosimetry can be made, including taking a fast exposure picture of the beam and comparing the beam radius captured in the micrograph with the one predicted by the dosimetry and verifying the Gaussian shape of the beam by profiling the beam with the peak density Faraday cup. Those checks give more confidence that any errors in the determination of the dose rates are small.

The first thing to notice is that at higher temperatures there is a *dose rate dependence* of the dose-to-amorphization. At temperature T_1 there is no dose rate dependence: amorphization occurs at the same dose for all radii. When the temperature is increased to T_2, there is a deviation from the straight vertical line indicating that the dose-to-

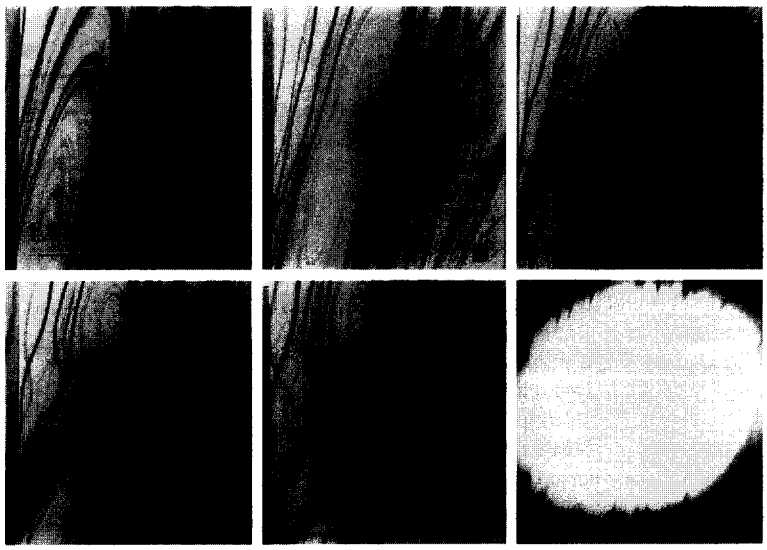

Fig. 4. Amorphization sequence during electron irradiation of Zr_3Fe at 200 K. At (A), the unirradiated material is shown; (B) after 960 s, bend contours start to thin and disappear; (C) after 1260 s, an amorphous spot is formed in the center of the beam; the amorphous spot grows in (D) (1980 s) and (E) (3180 s), but saturates at a size smaller than the beam size shown in (F).

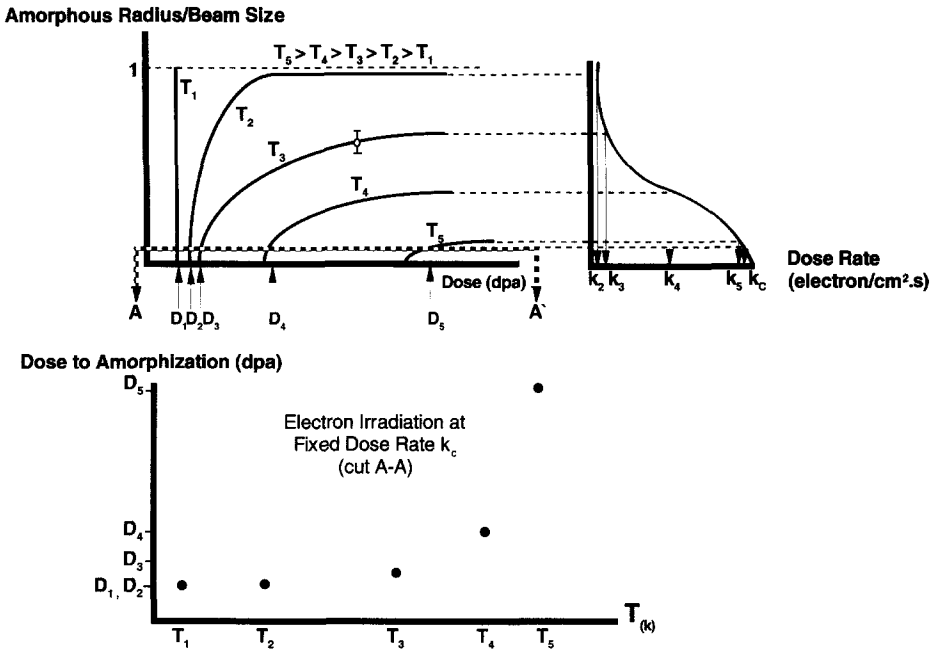

Fig. 5. Schematic plot of amorphous beam radius as a function of dose for several temperatures, showing influence of dose rate and relationship to dose-to-amorphization versus temperature curve.

amorphization is higher at lower dose rates. At temperature T_3 the rate of annealing is large enough that it can overwhelm damage production smaller than k_3, so k_3 is the *critical dose rate* for amorphization at temperature T_3. As can be seen from Fig. 5, the critical dose rate increases with temperature until it is higher than the peak dose rate in the beam. Above this temperature amorphization ceases to occur: that is the critical temperature for amorphization at the peak dose rate in the beam.

The curve shown in Fig. 2 can be obtained from Fig. 5 by performing the cut A–A, as shown in the lower part of Fig. 5. Performing such a cut means plotting the dose-to-

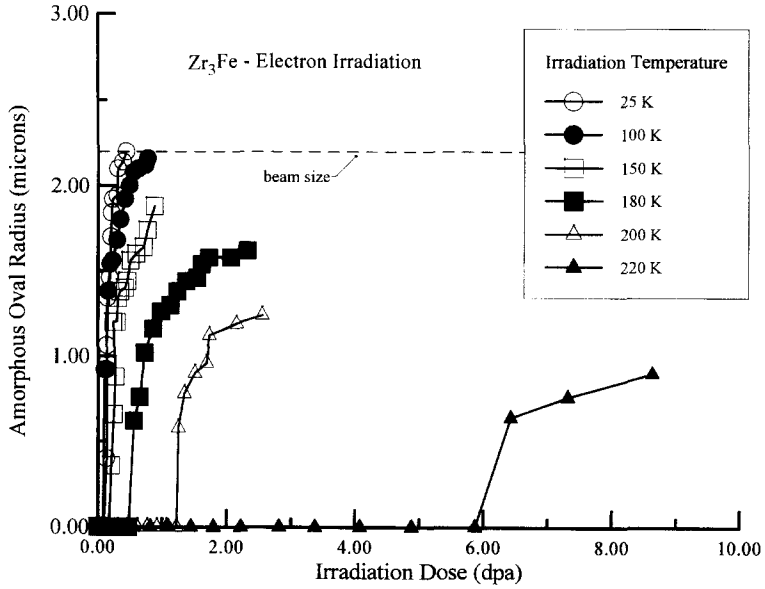

Fig. 6. Amorphous radius (μm) versus dose in displacement per atom, for amorphization of Zr_3Fe under 0.9 MeV electron irradiation at various temperatures. At higher irradiation temperature the critical dose rate for amorphization increases (the final size of the amorphous zone decreases).

amorphization for a fixed dose rate. The dose-to-amorphization versus temperature curve would be different if the cut A–A were performed at a larger radius (corresponding to a lower value of the dose rate), so using diffraction apertures of different size to gauge amorphization yields different results. Therefore reports of amorphization results should include the specification of the amorphous radius used as an amorphization gauge.

The dose for *the onset of amorphization* can also be obtained directly from Fig. 5. This dose gives a direct measure of the damage level that needs to be reached before amorphization can occur. Fig. 6 shows a typical set of data obtained for electron irradiation-induced amorphization of Zr_3Fe. A higher dose rate decreases the dose-to-amorphization, and increases the critical temperature, enlarging the amorphization domain [92]. Xu [93] demonstrated a similar dose rate effect at intermediate temperatures, but failed to detect the increase in the critical temperature. The method is shown in Fig. 6 where the size of the amorphous zone is plotted against irradiation time. By performing iso-dose rate cuts using the method above, it is possible to recover the usual dose-to-amorphization versus temperature graph but at various dose rates. This is shown in Fig. 8, where it is clear that the critical temperature increases with dose rate [94]. The decrease of the dose-to-amorphization with increasing dose rate has also been shown for Ar ion irradiation of Zr_3Fe [95]. After irradiating the material to a constant fluence of 10^{19} ion m^{-2}, amorphization is achieved at 1.47×10^{16} ion m^{-2} s^{-1} but not at 9×10^{14} ion m^{-2} s^{-1}. Dose rate effects under ion irradiation were also observed in amorphization of Si [54].

2.5.2. Crystalline fraction

The measurement of dose rate influence in Section 2.5.1 concerns states where amorphization either has or has nor occurred. It is possible to study the intermediary states as well, by measuring the crystalline fraction as a function of irradiation dose for different types of irradiation. This can be done by measuring the intensity of a crystalline diffracted spot from TEM micrograph negatives, or X-ray diffraction. This type of experiment coupled with TEM observations of the transformation morphology can help determine the amorphization mechanisms. Other techniques, such as RBS and Mössbauer, can indirectly measure amorphization fraction, but measuring diffraction intensity is the most direct technique available.

In this technique, it is possible to derive conclusions about amorphization mechanisms. Different results are shown in Fig. 7A. For example: if the curve follows *a*, then the material remains crystalline through most of the experiment, and amorphization occurs by a lattice instability near the end of the irradiation time after enough damage has accumulated. Curve *b* has been observed during amorphization of intermetallic precipitates under neutron irradiation [96]. The linear dependence of the amorphous fraction on dose indicates an interface controlled process as explained in Section 2.6.3 [97]. Curve *c* shows amorphization by cascade superposition: the curvature near the beginning is related to the need to accumulate some damage before cascade superposition becomes probable. Curves *d* and *e* show amorphization by direct cascade impact for cascades of different sizes. The curvature near the end of the irradiation time in *c*, *d* and *e* is caused by the increased probability of an impact of new cascades on already amorphous regions [14].

An example of such a quantitative measurement is shown in Fig. 7B, for amorphization of $Zr_2(Ni, Fe)$ precipitates in Zircaloy-2 under electron irradiation [89]. The crystalline fraction is measured by the normalized ratio of intensities of the diffracted spot to the transmitted spot, shown at the bottom of the picture. The crystalline fraction Ψ is experimentally defined as:

$$\Psi(t) = \frac{I_{hkl}(t)/I_{tr}(t)}{I_{hkl}(t=0)/I_{tr}(t=0)} \tag{1}$$

where $I_{hkl}(t)$ is the intensity of the diffracted beam *hkl* at time t, $I_{tr}(t)$ is the intensity of the transmitted beam at time t, and the denominator has the same quantities at the start of the irradiation. In order for the experiment above to work, the sample orientation has to be kept constant throughout the experiment. In the exact orientation condition shown in Fig. 7B the four primary diffracted spots decrease equally as the sample undergoes amorphization, showing that the specimen orientation does not vary during the experiment. Fig. 7C shows that the evolution of the parameter Ψ with dose most approximates curve *a* in this case .

Brillouin scattering experiments represent another window on the amorphization process, as they can provide information on the changes in elastic constants during ion bombardment of intermetallic compounds, by measuring their surface phonon velocity [98]. For compounds that become amorphous the phonon velocity (and therefore the shear modulus), decreases exponentially until the onset of amorphization, remaining constant thereafter. For the compounds that remain crystalline, a smaller change in shear modulus is noted. This shows that lattice softening precedes or accompanies amorphization.

In the context of the types of experiments described above, we now review the existing data on irradiation-induced amorphization of intermetallic compounds.

2.6. Experimental data on amorphization

There is a large body of experimental evidence on the amorphization of binary and ternary intermetallic compounds under irradiation [3,4]. Early experiments on amorphization under irradiation concentrated on structural factors affecting phase stability and on the development of general criteria to predict amorphization under irradiation

[5,99]. More detailed descriptions of amorphization undertaken in other studies [14,100,101], demonstrate the fundamental role of kinetics in predicting amorphization under the three different types of irradiation as described in the following sections.

2.6.1. Ion irradiation

Amorphization of intermetallic compounds under ion irradiation was first reported in Zr_3Al [85]. A detailed transmission electron microscopy (TEM) study of cascades and disordered zones, showed that amorphization occurs

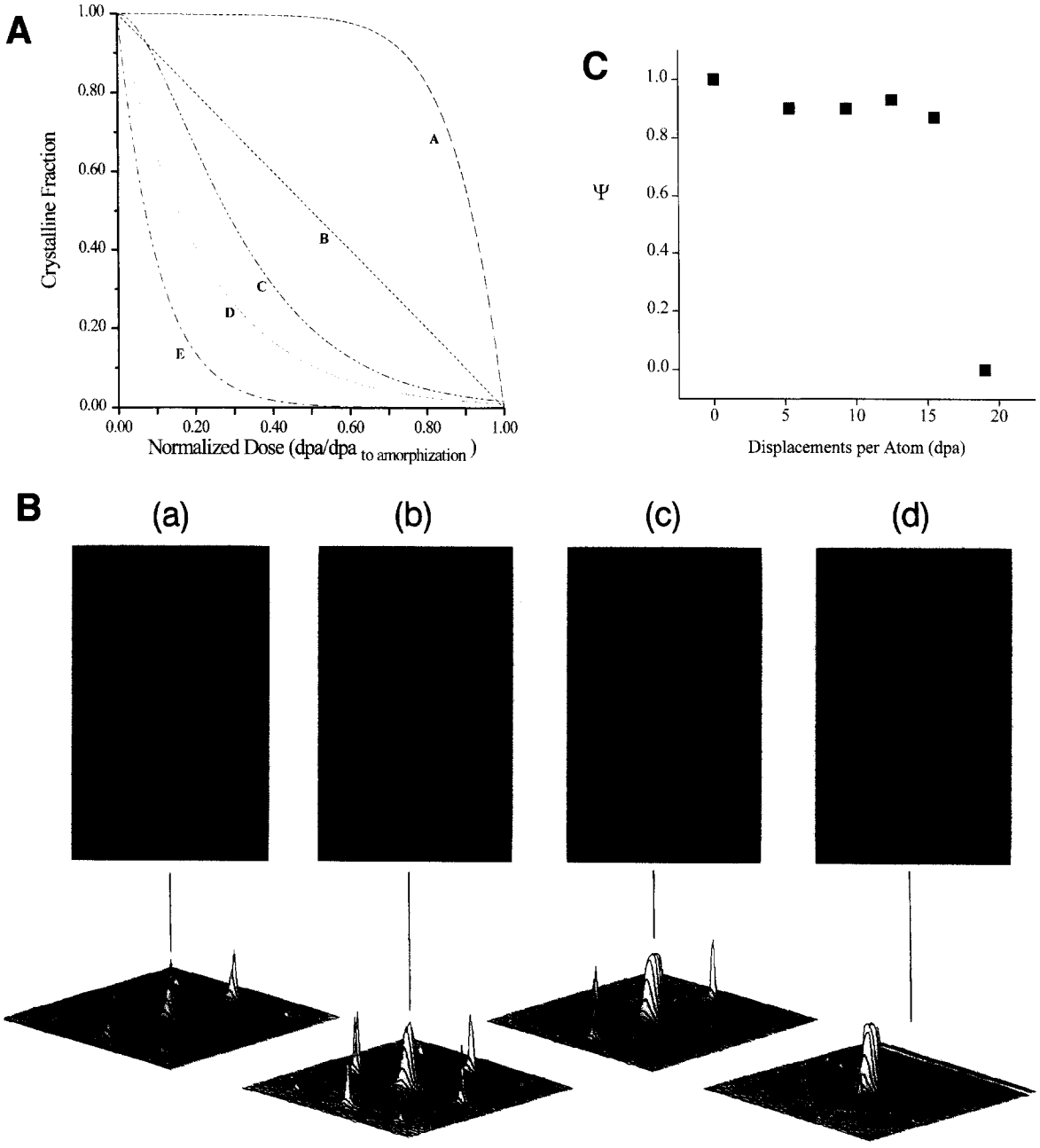

Fig. 7. A. Normalized crystalline fraction versus normalized dose (in $dpa/dpa_{amorphization}$) for different amorphization mechanisms (schematic): In *a* the transformation occurs abruptly, at the end of the irradiation time by a lattice instability, once enough damage has accumulated so that a percolation condition is reached; in *b* an interface-controlled process yields linear kinetics; in *c* amorphization occurs by cascade superposition, so a threshold is visible for the start of the process; in *d* and *e*, amorphization occurs by direct cascade impact for cascades of different sizes. The curvature at the end of curves *c*, *d* and *e* represents the decreasing probability of hitting an amorphous zone toward the end of the irradiation.B. Diffraction intensity plot sequence during amorphization of Zr_2(Ni, Fe) under electron irradiation [89].C. Normalized crystalline fraction as a function of dose measured from the data shown in B.

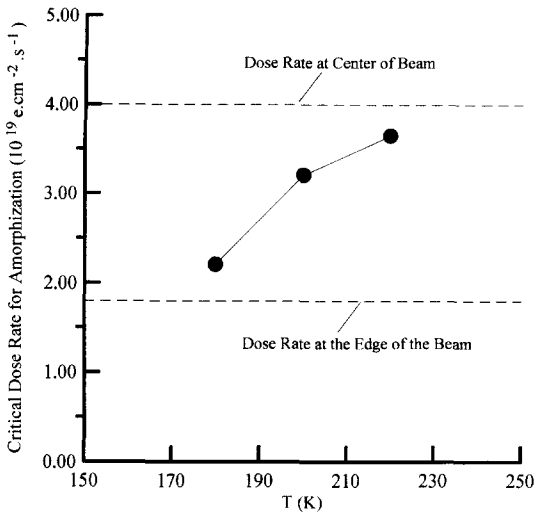

Fig. 8. Critical dose rate for amorphization of Zr_3Fe under electron irradiation as a function of temperature. Also shown is the dose rate variation afforded within the electron beam. [94]

by an accumulation of defects surpassing a critical defect density for amorphization, rather than by direct amorphization in the cascades. However, since electron irradiation fails to render the material completely amorphous even at very high doses, cascades are necessary for amorphization in that case.

Ion irradiation being readily available, many survey-type experiments were conducted. Experiments show that while many compounds are susceptible to amorphization under ion irradiation several others are not. Considerable experimental effort identified which compounds undergo amorphization [13,99,102,103] or crystallization [104], under standard conditions and correlated amorphization susceptibility with material properties common to the ensemble of compounds that amorphize. Examples of material properties used in these correlations are the intermetallic compound place in the phase diagram (near a deep eutectic), width of the intermetallic phase field (narrow phase field is more susceptible to amorphization), melting temperature (the critical temperature is proportional to the melting temperature) and complexity of structure (more complex structures are more susceptible to amorphization). Although empirical in nature, some of these criteria such as width of phase field and complexity of structure can be related to more physical parameters such as anti-site defect energy and the kinetic difficulty of re-forming complex structures after destruction by irradiation [3].

The role of ion mass on amorphization was studied by Koike et al. [81] and Nastasi et al. [105] who found different critical temperatures for amorphization under electron and ion irradiation in CuTi and Ni_2Al_3. Detailed kinetic studies on the role of ion mass on amorphization were conducted by Jaouen and co-workers, who measured the amorphous fraction in NiTi and NiAl as a function of dose for different types of ions [6,106]. They analyzed their results using the model developed by Gibbons [107] who gives the relationship between amorphous volume fraction and dose as:

$$C_{\mathrm{am}} = 1 - \sum_{i=0}^{n-1} \frac{(a\phi t)^i}{i!}[\exp(-a\phi t)] \tag{2}$$

where a is the damage cross section, ϕt is the ion fluence and n is the number of cascade overlaps required for amorphization. For low energy heavy ions the amorphization kinetics could be described by $n = 1$ (direct amorphization), while for higher energy and lighter ions, n is equal to 2 or higher.

In the Ni–Al system simultaneous electron and ion irradiation results in a higher dose-to-amorphization than either of the two irradiations by themselves [108], as is the case in Si [58]. This is due to the availability of freely migrating defects from electron irradiation helping anneal the ion damage. These results clearly show that the irradiation conditions are crucial in determining whether a compound will amorphize or not.

There have been several studies of the influence of ion species on amorphization. Those studies typically utilize the noble gases as irradiating particles in order to minimize chemical effects of the implanted species on the phase stability of the compound. The presence of displacement cascades in ion irradiation greatly extends the temperature range where amorphization is possible relative to electron irradiation. The difference in critical temperature between ion and electron irradiation is typically 300 K [90] as seen in Fig. 3. The reason for this difference is that the local damage rates within the cascades are higher than what can be achieved by electron irradiation, and the available annealing mechanisms are correspondingly less effective. It follows then that different ions, producing displacement cascades of different density, have different effects on phase stability.

Koike et al. [109] irradiated Zr_3Al with electrons, Ne, Kr and Xe ions, finding a difference of 200 K between the critical temperatures for electron and Ne ion irradiation, a further increase of 50 K when using Kr, but no further increase when using Xe. The authors attributed this saturation to approaching the glass temperature of the solid, T_g. Howe et al. [90] irradiated Zr_3Fe with different types of ions and showed that amorphization susceptibility can be correlated with average deposited energy density in the cascade through the parameter $\overline{\theta_\nu}$, given by:

$$\overline{\theta_\nu} = \frac{0.2\nu(E)}{N_\nu V_{\mathrm{R}}} \tag{3}$$

where $\nu(E)$ is the nuclear energy loss, N_ν is the number of atoms in a spheroid determined by the x and y components of straggling and V_{R} is the ratio of the amorphous volume to the total volume of the cascade. In general the denser the cascades, the easier it is to amorphize a mate-

rial. At high deposited energy densities (often corresponding to low ion energies) the amorphization probability is high. At lower values of $\overline{\theta_c}$, there is an increasing tendency for multiple damaged regions to form within a cascade.

2.6.2. Electron irradiation

The observation of amorphization of intermetallic compounds under electron irradiation demonstrated that amorphization could be achieved even in the absence of collision cascades [110,111]. Only partial amorphization of Zr_3Al is achieved under electron irradiation even at high doses (44 dpa) [85]. Zr_3Al has an unusually low critical temperature for amorphization under electron irradiation [4]. Another study showed that Zr_3Al only amorphizes under electron irradiation if the TEM sample is prepared by electrochemical polishing [112], (which possibly introduces hydrogen into the sample).

Except for preferential amorphization in the vicinity of defects such as dislocations [113] and grain boundaries [114] (treated in more detail in Section 2.7.2), amorphization by electron irradiation occurs *homogeneously*, by a combination of chemical disordering and an increase in point defect concentration. Since metallic solid solutions do not amorphize under irradiation, the role of chemical disordering appears to be important. The experiments of Luzzi et al. in the CuTi system [115], confirm this since they show a sharp decrease in the amount of chemical disordering attainable at the same temperature at which the rate of amorphization also sharply decreases. This implies a direct relation between a reduced amount of chemical disorder and absence of amorphization. However, this clear relationship is not always present: there is considerable evidence for the need for an additional contribution from point defect accumulation to the amorphization process [8,116]. Hence, chemical disordering is a necessary but not sufficient condition for amorphization under electron irradiation [8,117,118].

As in the case of ion irradiation, for a given set of irradiation conditions some compounds are susceptible to amorphization under electron irradiation and others are not. The subset of 'amorphizable' compounds under electron irradiation is smaller than that for ion irradiation [119]. It has also been shown that under electron irradiation, the dose-to-amorphization decreases [120,121], and that the critical temperature increases with dose rate: each critical temperature corresponds to a critical dose rate for amorphization [91]. This again points to the role of kinetics in the amorphization process. The time from the onset of amorphization to the end of the transformation is small compared to the total irradiation time [89], which indicates that damage accumulation is the rate-controlling process for amorphization.

2.6.3. Neutron irradiation

Neutron irradiation can cause damage either directly by collisions of fast neutrons with the atoms in the material causing displacement cascades, or indirectly by inducing (n, γ) reactions or nuclear fission, and relying on the γ recoils or on the fission fragments to create displacements. The first case constitutes neutron irradiation proper, and the second is more properly classified as ion irradiation by fission fragments and recoils. Fission fragment irradiation provided the first reported example of amorphization of an intermetallic compound, U_6Fe [122], the kinetics of which were later studied in detail [100].

Only a few examples of fast-neutron-induced amorphization have been reported [4], notably on A15 compounds. Mo_3Si [123] and Nb_3Ge [124]. Also, the compound Fe_3B amorphizes under neutron irradiation [125]. Additionally, intermetallic compounds present in commercial alloys amorphize during neutron irradiation. The Laves phase Fe_2Mo found in a Fe–Ni–Cr Mo alloy amorphizes after a fluence of 7×10^{26} n m^{-2} at 723 K [126]. The relative lack of reported instances of neutron-induced amorphization is due to the relatively few irradiations of bulk intermetallic alloys conducted, and to amorphization of second phase particles in alloys often not being the main interest of the research [127,128].

More recently, the ternary intermetallic precipitates $Zr(Cr, Fe)_2$ and $Zr_2(Ni, Fe)$ have been observed to amorphize at low temperature (350 K) [129,130]. At 560 K, the $Zr_2(Ni, Fe)$ precipitates are crystalline while the $Zr(Cr, Fe)_2$ precipitates exhibit a duplex structure consisting of an amorphous layer that starts at the precipitate–matrix interface and whose thickness increases linearly with fluence (Fig. 9). The amorphous phase is also severely depleted in Fe. This phenomenon has been explained by a model in

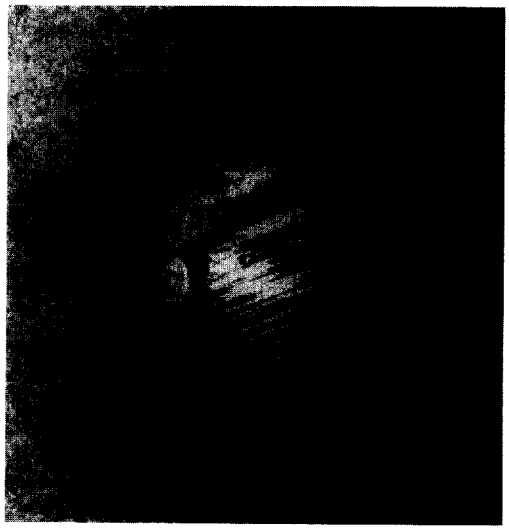

Fig. 9. $Zr(Cr, Fe)_2$ precipitate in Zircaloy, after irradiation to fluence of 4×10^{25} n m^{-2} in BR3 reactor. The amorphous layer (A) forms at the precipitate-matrix interface and gradually moves into the crystalline core (C) until the whole precipitate is amorphous (photo courtesy of C. Regnard, CEA).

which ballistic mixing drives the compound away from stoichiometry and thereby facilitates amorphization at the interface [97]. Under electron and ion irradiation those same precipitates do not exhibit preferential amorphization at the precipitate–matrix interface [96,129,130]. Under Ar ion irradiation, the $Zr(Cr, Fe)_2$ precipitates in Zircaloy amorphize at temperatures up to 650 K (without Fe depletion) and the $Zr_2(Ni, Fe)$ precipitates do so at least up to 600 K [131], while under electron irradiation, both types of precipitates remain crystalline above an irradiation temperature of 300 K. Other compounds found in new Zr-based alloys also amorphize under neutron irradiation [132].

Extensive neutron amorphization experiments have also been conducted on the U–Si system by Birtcher and co-workers [133,134], who report amorphization of U_3Si during neutron irradiation at room temperature, but not at 623 K, after fission fragment irradiation to 0.08 dpa. Accompanying the transformation, lattice parameter contractions were observed both in the a and c directions of the tetragonal unit cell.

The main conclusion from this data is that it is not possible to define a susceptibility to amorphization under irradiation without specifying the irradiation conditions in detail. The irradiation conditions and the total dose received determine whether a compound amorphizes or not. Hence, amorphization susceptibility is not simply a material property, but depends on the irradiation conditions.

2.7. Other irradiation parameters

In addition to the irradiation particle type, irradiation dose and dose rate, other parameters affect amorphization under irradiation, including the presence of extended defects, compound stoichiometry and specimen orientation. Those are reviewed in the following.

2.7.1. Influence of compound stoichiometry

Intermetallic compounds usually exist in a narrow range of stoichiometry, since any departure from exact stoichiometry has to be accommodated either by structural vacancies or by anti-site defects, at great energy cost. The calculated free energy versus composition curve for $ZrFe_2$ shows that a small deviation from stoichiometry causes a large increase in free energy. There is evidence that intermetallic compound stoichiometry influences amorphization, although there have been no systematic attempts to study it.

A marked difference in amorphization susceptibility exists between $Cu_{0.48}Ti_{0.52}$ and $Cu_{0.52}Ti_{0.48}$ [135]. As mentioned above, the amorphization of $Zr(Cr, Fe)_2$ precipitates in Zircaloy under neutron irradiation is attributed to a departure from stoichiometry, induced in this case by ballistic mixing at the precipitate–matrix interface [97]. The Cr/Fe ratio also influences amorphization under neutron irradiation in $Zr(Cr_{1-x}, Fe_x)_2$ [96]. An investigation of the influence of x on the amorphization of $Zr_3(Fe_x, Ni_{1-x})$, shows no effect [136].

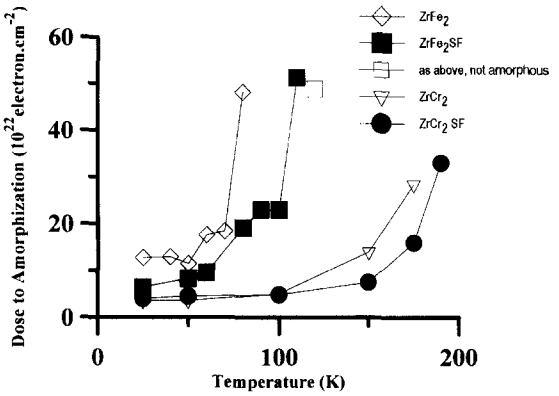

Fig. 10. Dose-to-amorphization versus temperature for $ZrCr_2$ and $ZrFe_2$ under electron irradiation, showing the effect of a high density of stacking faults (filled spots) on the amorphization process.

2.7.2. Influence of extended defects

The presence of extended defects such as dislocations, stacking faults and anti-phase boundaries has been shown to facilitate amorphization [113,114,137]. These studies detected preferential amorphization at dislocations in NiTi during electron irradiation at 160 K [113], twin boundaries in NiTi [137] and antiphase boundaries in Cu_4Ti_3 [114]. Preferential grain boundary amorphization under electron irradiation was recently demonstrated in spinel and coesite [34]. Preferential amorphization in thinner regions of the foil during electron irradiation of NiTi was noted by Thomas et al. [111].

The influence of stacking faults on amorphization of $ZrFe_2$ and $ZrCr_2$ under electron irradiation was determined by irradiating samples of each compound containing two phases, one with a larger stacking fault density than the other [136]. The results are shown in Fig. 10. The critical temperature of both compounds is approximately 15 K higher in the high stacking fault density phase. For $ZrFe_2$ the critical dose is twice as small in the high stacking fault phase than in the low density stacking fault phase, while in $ZrCr_2$, the critical doses are the same for both phases. There is a step in the dose-to-amorphization curve of $ZrFe_2$–SF that corresponds to the critical temperature of $ZrFe_2$.

The decrease in the critical dose is understandable by noting that the lattice strains associated with the extended defect cause amorphization to be easier near the defect as discussed below. Nastasi and Mayer [3] calculated the local increase in free energy at defects and concluded that this explained the preferential amorphization at dislocations. The change in the critical temperature is likely due to a change in migration energy or migration mode of the defect associated with the presence of the stacking faults.

2.7.3. Influence of specimen orientation

The orientation of the thin foil specimen under electron irradiation influences amorphization susceptibility. This

orientation dependence of amorphization is likely caused by the change in displacement energy with crystalline orientation. Electron irradiation of Zr_3Fe at energies below 400 keV also showed an orientation dependence of amorphization in the elongation of the amorphous spot along bend contours [138]. At 250 keV, the irradiation of a triple joint of three Zr_3Fe grains produced amorphization in one grain but not in the other two, as shown in Fig. 11 [91]. Xu [93] reported different dose-to-amorphization versus temperature curves in CoTi under electron irradiation, depending on the crystalline orientation.

Mori et al. [112] have shown evidence of preferential amorphization of Zr_3Al along bend contours around a deformation center, during electron irradiation at 160 K. The appearance of the amorphous zone in that case consists of an amorphous spot with amorphous tentacles emanating from it. As mentioned above, amorphization in this case is partly related to the type of sample preparation used. Similar effects of sample preparation were reported elsewhere [139].

2.7.4. Use of amorphization to study solid-state phenomena

Another type of amorphization experiment is shown in Fig. 12. Here the dose-to-amorphization in Zr_3Fe at a fixed temperature of 30 K is measured at several electron energies, at constant lattice orientation [138]. The temperature is kept low so thermal annealing does not affect the process. As the electron energy decreases, the maximum energy imparted to the lattice atoms also decreases, until the maximum energy transferable from the electrons to the atoms in one of the sublattices falls below the displacement threshold E_{d1} so that displacements can be initiated only in the other sublattice. As the energy is further decreased, a second threshold E_{d2} is reached below which neither atom can be directly displaced. Below this energy, displacements can only occur via a secondary displacement mechanism, where an electron displaces an impurity atom which can in turn cause a lattice displacement [138].

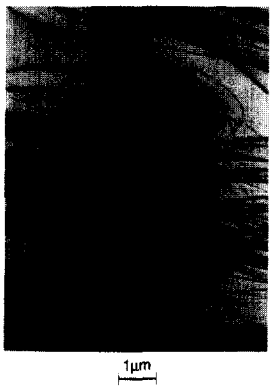

Fig. 11. Triple joint between three Zr_3Fe grains showing preferential amorphization during electron irradiation at 250 keV at 25 K.

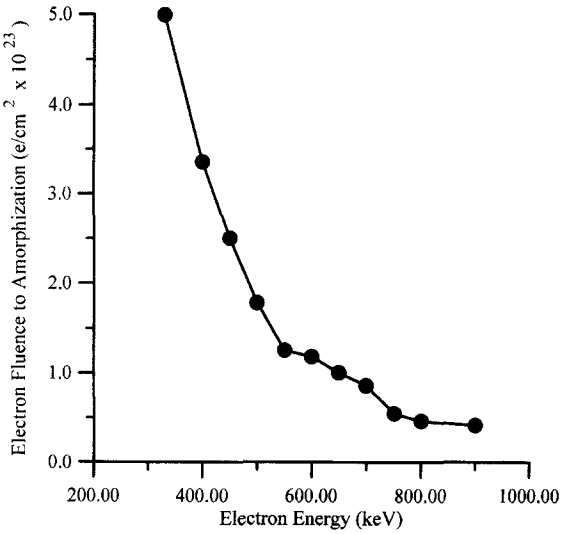

Fig. 12. Energy dependence of the dose-to-amorphization in $ZrCr_2$ during electron irradiation at 25 K.

Since the concentration of impurity elements is quite low, the amorphization doses are correspondingly much higher at energies below E_{d2}. The analysis of such experiments noting the electron energies at which transitions occur in the dose-to-amorphization allows a verification of the displacement energies for each of the sublattices [140]. Results have been obtained for the compounds Zr_2Fe, $ZrCr_2$ and Zr_3Fe [141]. Similar studies on the dependence of amorphization on electron energy have been conducted in non-metallic systems [32,142].

3. Theoretical analysis

The preceding experimental knowledge needs to be placed in the context of a theoretical model that provides basic understanding of the process. It is possible to describe amorphization susceptibility or tendency with various empirical criteria, mentioned in Section 2.6.1. Some of the limitations of these criteria have been discussed before [7]. In addition to these it is important to mention the criterion of Egami and Waseda [143] who use atomic size to determine the range of formability of metallic glasses from a solid solution. Such criteria have also been derived from simulations of glass formation [144]. As discussed below, this does not apply to a case where the starting material is an intermetallic compound.

A more mechanistic understanding of amorphization under irradiation is clearly desirable. The following discussion of theoretical models of amorphization aims at developing such an understanding. A few general observations based on the experimental observations discussed in Section 2 help orient this theoretical discussion on amorphization under irradiation.

(1) Amorphization occurs only below a critical temperature and only after a critical dose is reached.

(2) Amorphization under irradiation is easier at low temperature than at high temperature.

(3) Once the amorphous phase is formed, it does not evolve further; that is, the amorphous phase is stable under irradiation.

(4) The more severe the irradiation damage, the higher the critical temperature for amorphization.

These four observations can be rationalized in terms of a model that states that the amorphous phase can be formed when the accumulated irradiation damage is higher than a critical level of damage. For amorphization to occur,

$$D(t) > D_{\text{crit}} \tag{4}$$

where $D(t)$ is the damage as a function of irradiation time and D_{crit} is the critical level of damage. The accumulation of damage is written as;

$$D(t) = [G - A(T)]t \tag{5}$$

where G is the displacement rate (dpa s^{-1}) and $A(T)$ (s^{-1}) is the temperature-dependent annealing rate. The annealing rate $A(T)$ is written in general form as:

$$A(T) = \sum_i \alpha_j C_j v_j \exp(-E_j/kT), \tag{6}$$

where i stands for all annealing defects, C_i is the concentration of the defect producing annealing and E_i its migration energy. Eq. (6) implies the annealing rate overwhelms damage production at high temperatures. At low temperature the damage rate is higher than the annealing rate. If the annealing rate is too high, as in the case of pure metals, amorphization never occurs. The annealing rate increases with temperature until, at the critical temperature, it becomes higher than the damage rate. Hence, the critical temperature is found from:

$$A(T_c) = G \tag{7}$$

At the critical temperature the damage rate goes to zero and the time to amorphization goes to infinity. According to the model, if a suitable way exists to quantify the accumulation of damage and to determine the critical level of damage, then the dose-to-amorphization can be predicted. Once Eq. (4) is satisfied, then amorphization can occur.

To predict amorphization behavior, four questions based on the four observations above need to be answered:

(1) What is the critical level of damage for amorphization?

(2) How fast is the critical damage level for amorphization reached under given irradiation conditions?

(3) Once the critical level is reached, how does amorphization actually occur (e.g. elastic instability, homogeneous nucleation of amorphous zones, amorphization within cascades, etc.)?

(4) After the material is amorphized, why is it stable under further irradiation?

The first two questions, of how to determine the critical level of damage and how to calculate the rate of damage accumulation, have received the greatest attention in the literature. We review the work on question (1) in Section 3.1, question (2) is reviewed in Section 3.2, and questions (3) and (4) are discussed in Sections 3.3 and 3.4 in the context of a new model (presented in Section 3.4).

3.1. Critical damage level

As pointed out by Martin [145,146] and Russell [147] phase transformations under irradiation are not governed by the same rules as phase transformations that occur under purely thermal conditions. This is because the constant bombardment of particles causes several of the conditions necessary for thermodynamic equilibrium to be violated. In particular, the irradiating particles represent an energy input to the system. By impacting the atoms in the solid, the irradiating particles cause atomic displacements, replacements and displacement cascades, all of which are absent outside irradiation. Because of this, it is possible only to determine a steady state under irradiation, but not a true equilibrium.

In particular, this means that the criterion for phase stability valid outside irradiation (the minimization of the Gibbs free energy), is not necessarily applicable to phase transformations under irradiation [148]. To predict phase stability under irradiation the preferred approach is to develop a functional that would replace the Gibbs free energy, incorporating the effects of ballistic jumps as well as thermal jumps. Such potentials have been constructed by Bellon and Martin and co-workers for specific cases such as radiation-induced disordering and radiation-induced precipitation and dissolution [149]. Some of the simplifications of their models have interesting physical results such as the application of the regular solution model, showing that the effect of irradiation is equivalent to a temperature increase (law of corresponding states) [148]. If, for example, this result had been found for an amorphization reaction, it could be physically argued that radiation drives the effective temperature up into the liquid region which is similar to the amorphous structure.

However, there is not a general potential applicable to all irradiation driven processes, and in particular, there is not one for amorphization. One way to circumvent this problem is to use a modified free energy that takes into account the energy increase brought in by the increase in both point defects and chemical disordering [150]. Although not formally correct, the advantage of this approach is that such a potential can be directly related to quantities such as the point defect concentrations and to the Bragg–Williams long-range order parameter S [151], which can be calculated from the experimental conditions to various degrees of sophistication [152].

3.1.1. Modified free-energy criterion

Following this approach, it is possible to use the modified free energy as a measure of phase stability [89,152,153]. The condition for amorphization then becomes

$$\Delta G_{\mathrm{irr}} > \Delta G_{\mathrm{ca}} \tag{8}$$

where

$$\Delta G_{\mathrm{ca}} = G_{\mathrm{c}} - G_{\mathrm{a}} \tag{9}$$

is the difference in free energy between the crystalline and amorphous phase and

$$\Delta G_{\mathrm{irr}} = G_{\mathrm{irr}} - G_{\mathrm{unirr}} = \sum_i \Delta G^i_{\mathrm{irr}} \tag{10}$$

is the difference in free energy between the irradiated and unirradiated solid. Here ΔG_{irr} is the free energy change due to all the possible mechanisms of energy storage in the solid such as the creation of point defects, increase in chemical disorder, presence of dislocation, stacking faults, etc.

Assuming that the different processes of defect accumulation are independent of each other and making approximations such as using the Bragg–Williams description of long-range order (LRO) to calculate the free energy change to disorder, it is possible to evaluate ΔG_{irr} and compare it to ΔG_{ca} [152]. The change in free energy with irradiation is written as:

$$\begin{aligned}\Delta G_{\mathrm{irr}} &= \Delta G_{\mathrm{def}} + \Delta G_{\mathrm{dis}} \\ &= \sum_i \left[C_i E_i - T\Delta S_i\right] + \Delta C_{\mathrm{pab}} N\Omega - T\Delta S_{\mathrm{dis}}\end{aligned} \tag{11}$$

where S is the Bragg–Williams long-range order parameter, C_i is the concentration of defect i, E_i its formation energy, N is the number of lattice sites per mol, Ω is the ordering energy. ΔS_i the configurational entropy change from introducing point defects and ΔS_{dis} is the configurational entropy change due to the introduction of anti-site defects [151]. The change in the number of A–B pairs per mol as a result of changes in S is

$$\Delta C_{\mathrm{pab}} = N\left[A(1-S^2) + B(1-S)\right] \tag{12}$$

where A and B are constants that depend on the crystal structure. It is important to note that the configurational entropy as calculated here is only defined in the crystalline phase. The concentration of defects and the order parameter can be calculated using chemical rate theory as explained in Section 3.2 [152,153] and the several order–disorder kinetics expressions available [155–157].

With this approach, it is possible to model the whole dose-to-amorphization versus temperature curve, as well as the kinetics of amorphization. Both the critical temperature and the critical dose are derived naturally from the model. One problem with this approach, is that although the amorphization process is clearly cooperative, no interaction between defects is explicitly assumed.

3.1.2. Global damage criteria

Other criteria have also been proposed to evaluate the critical damage level for amorphization. The more developed model is the modified Lindemann criterion proposed by Lam and Okamoto [10]. They proposed at first that volume expansion be considered the critical variable governing amorphization [4,158], that is, at a critical volume expansion, the crystal becomes unstable relative to the amorphous phase and amorphization occurs. The volume expansion can be caused by point defects, or chemical disorder, and the authors related it to the lattice softening measured by Brillouin scattering [119]. Computer simulations showing that amorphization does not occur even at large volume expansions, led the authors to propose a different model based on the Lindemann criterion for melting [159] (although a recent paper found amorphization by volume expansion if there is some anisotropy in the forces applied [160]). The modified Lindemann criterion states that amorphization (referred to as solid-state melting) occurs when

$$\langle x^2 \rangle > \langle x^2_{\mathrm{crit}} \rangle \tag{13}$$

where $\langle x^2 \rangle$ is the mean square static displacement of the atoms in the solid from their equilibrium lattice positions and $\langle x^2_{\mathrm{crit}} \rangle$ is the critical mean square displacement at melting. According to this model, amorphization can be seen as solid state melting: a high defect concentration softens the lattice and reduces the melting temperature.

The advantage of this approach is that it reduces the different damage contributions to a single parameter. For example, when an anti-site defect is created, there is a lattice distortion due to the insertion of the 'wrong' atom in the sublattice, which translates to a local strain, increasing $\langle x^2 \rangle$. In the same way, the effects of thermal motion, point defect creation, are grouped under the same parameter. Molecular dynamics computer simulations show that amorphization always occurs at a fixed value of $\langle x^2 \rangle$ whether the origin of the increase in mean square displacements is point defects, antisite defects or thermal motion. In those simulations, because it is difficult to calculate $\langle x^2 \rangle$ due to the difficulty of determining where the lattice was, the dispersion in the nearest neighbor distance is used as the parameter. The dispersion in nearest neighbor distance is related to $\langle x^2 \rangle$ and correlates well with amorphization [10], since the nearest neighbor distances in a crystal are constant from atom to atom while, by definition, an amorphous solid has a range of nearest neighbor distances.

Another interesting feature of this model is that it predicts that the enthalpy difference between the crystal and the amorphous phases, ΔH_{ca} can be estimated as:

$$\Delta H_{\mathrm{ca}} = \Delta H_{\mathrm{f}}\left[1 - \left(\frac{\Theta^{\mathrm{a}}_{\mathrm{D}}}{\Theta^{\mathrm{c}}_{\mathrm{D}}}\right)^2\right] \tag{14}$$

where ΔH_{f} is the enthalpy of fusion, and $\Theta^{\mathrm{a}}_{\mathrm{D}}$ and $\Theta^{\mathrm{c}}_{\mathrm{D}}$ are the Debye temperatures of the amorphous and crystal. Eq.

(14) predicts that as the ratio of the Debye temperature of the amorphous solid to the crystalline solid increases, ΔH_{ca} decreases and, as a consequence, the amorphization tendency increases. This has been shown for the Zr–Ni system [161] and for the Zr–Fe system [162]: in both systems the compounds that have the higher Debye temperatures are the most difficult to amorphize.

While this theory can predict amorphization during computer simulations, it is difficult to use in practical under experimental conditions, since the quantities on which it is based ($\langle x^2 \rangle$ and nearest neighbor dispersion), cannot be measured directly. The mean square displacement can only be measured indirectly by measuring the Debye–Waller factor obtained for example from EXAFS measurements (extended X-ray absorption fine structure). The same problem occurs with the criterion proposed by Kulp and co-workers [16], which uses atomic level average shear stresses as an amorphization gauge. While their criterion can be applied in molecular dynamics simulations, experimental verification rests on the development of an adequate atomic probe that can give information about the atomic level quantities they use.

A more fundamental problem is that while it is clear that a solid with $\langle x^2_{crit} \rangle$ is amorphous, it is not clear whether amorphization results from arriving at $\langle x^2_{crit} \rangle$ or vice-versa. Certainly it is possible to find characteristics of the amorphous structure such as mean square displacement, or dispersion in the nearest neighbor distance that only reach a certain critical value in the amorphous structure. Measuring $\langle x^2 \rangle$ can provide a gauge to detect when amorphization occurs, i.e. Eq. (13) is satisfied *after* amorphization. Thus, although there is a correlation between $\langle x^2_{crit} \rangle$ and amorphization, there may not be a causal relationship. This would make the criterion a *description* of the process, rather than a *prediction* of the process.

This model is also not intended to predict amorphization kinetics. It is possible of course, to calculate $\langle x^2 \rangle$ by models similar to the one expressed in Eqs. (8)–(11) relating the point defects and chemical disorder to the mean square displacement. In that case these models would be an alternative to using the modified free energy for estimating the critical defect concentration for amorphization.

3.1.3. Amorphization and melting

Other theories applicable to the melting transition have been used to describe amorphization in the solid state by irradiation. One interesting approach was used by Li and co-workers [163] who proposed a Landau theory of the crystal to glass transition based on the interactions of static defects with the overall order parameter. Fecht [164] presented calculations showing that a high concentration of defects such as vacancies, interstitials or anti-site defects effectively reduce the melting temperature of the solid. At higher defect concentrations the liquid appears at successively lower temperatures until below the glass transition temperature an amorphous phase appears. The calculations show that the absolute defect limit for solid stability in Al is 0.077 vacancies. This is of course much higher than defect concentrations achievable in metals even during irradiation. The glass transition temperature represents the maximum limit of stability for the glassy phase, so that above T_g not even irradiation will cause amorphization. Although the model is presented as applicable to irradiation-induced amorphization, in reality kinetic considerations preclude amorphization from occurring at temperatures above T_c, which is smaller than T_g. So the stability limit of 0.077 defect concentration should be regarded as an absolute limit which is seldom, if at all, reached in practice. In the same way, the glass transition temperature represents the locus of the points above which any remnant amorphous phase transforms to a crystal. In effect the annealing mechanisms activated at T_c do not allow the amorphous phase to reach T_g. Thus, this criterion has limited ability to predict amorphization behavior under practical irradiation conditions.

Granato [165,166] has recently proposed that by considering the interstitialcy (dumbbell arrangement) as the basic structural unit of amorphous materials or liquids it is possible to explain several characteristics of these materials such as the decreasing specific heat with increasing temperature of metals in the liquid state [165]. Granato derives from this an equivalent Lindemann criterion to predict melting, and uses the model to determine the structure of amorphous solids from the radial distribution function and the vibrational density of states obtained from inelastic neutron scattering, finding good agreement with experiment [166]. Specific defect characteristics of pure metals, such as the ratio of entropy changes and volume changes upon melting (amorphization) are given as reasons for developing the model [165]. The arguments are developed however for the melting of pure metals which do not undergo amorphization under irradiation. However, defect configurations are much different in intermetallic compounds [167], so the reasons for developing such a model have to be demonstrated for the type of system that undergoes amorphization under irradiation.

3.2. Damage accumulation mechanisms

The other half of the problem is to calculate the rate of damage accumulation, while taking concurrent annealing into account. One crucial observation is that since the dose-to-amorphization decreases with temperature, long-range diffusion hinders rather than helps the amorphization process. Thus, the actual amorphization process is effected without long-range atomic rearrangements, occurring instead by local atomic rearrangements, possibly within the unit cell.

The annealing stages observed in Figs. 2, 3 and 9 are the result of the motion of different defects activated at different temperatures. In a binary intermetallic compound

there are at least six different types of defects: vacancies on either sublattice, interstitials of both types of atoms, and anti-site defects in both sublattices. The migration and formation energies of these compounds are crucial to determining the dose-to-amorphization (for example their migration energies have to correspond to the critical temperatures observed). In the study conducted by Shoemaker and co-workers [167], it is found that Cu interstitials migrated easily in the two-dimensional mode within the Cu planes ($E_m = 0.2$ eV), and very seldom cross Ti planes ($E_m = 1$ eV). However, when an anti site defect is present in the Ti planes, it acts as a 'gateway' to Cu interstitials by lowering the migration energy across Ti planes to 0.6 eV. This enables interstitial-induced reordering to take place. This type of synergistic interaction between chemical and topological disorder should be expected in intermetallic compounds, and makes the problem of calculating damage accumulation more complex than in pure metals. A further complicating factor is that the defect energies change as damage accumulates [5]. For example the ordering energy goes to zero as long-range order is lost. It is however, important to note that the critical temperatures are determined by the migration energies in the *undamaged* compound. Although this model gives a simple picture of the temperature dependence of amorphization for the case of homogeneous damage as caused by electron irradiation, when directly applied this model gives unphysically low activation energies. The likely reason is that the actual damage accumulation process is more complex than outlined above, since the Cj also depend on G and T. This can cause a more complicated dependence of the critical temperature on defect migration energies than expressed in Eq. (6). For example the model developed in [152] found that the critical temperature corresponded to half the interstitial migration energy because the experiment was conducted in the recombination-dominated regime. A proper approach to modeling amorphization will thus yield the physical meaning of the activation energy. For cascade-producing irradiation (ion and neutron) the processes that determine the critical temperature are related to cascade annealing and recrystallization, so these have to be modeled in addition to the above considerations.

According to rate theory, the defect concentrations are given by the coupled balance equations:

$$\frac{\partial C_v}{\partial t} = D_v \nabla^2 C_v + G - K_{iv} C_i C_v - \sum_j K_{jv} C_j C_v \qquad (15)$$

$$\frac{\partial C_i}{\partial t} = D_i \nabla^2 C_i + G - K_{iv} C_i C_v - \sum_j K_{ji} C_j C_i \qquad (16)$$

where C_i and C_v are the vacancy and interstitial concentrations, D_i and D_v their diffusion coefficients, K_{ji} and K_{jv} their respective annihilation rates at sinks type j, K_{iv} the recombination rate, G the displacement rate, and C_j the concentration of sink j.

These equations have been used to predict irradiation phenomena in alloys, and have been applied to the amorphization problem [92,152,153]. For example under irradiation conditions used during electron irradiation in a TEM steady state is not reached and a recombination-dominated regime exists for the whole irradiation time [152]. When one type of defect is much faster than the other, the foil surfaces dominate defect annihilation creating a supersaturation of the slow defect in the material [89], making amorphization possible.

Although Eqs. (15) and (16) have been used to predict amorphization in intermetallic compounds in the examples above, the rigorous application of rate theory to ordered compounds has not yet been achieved. The difficulty in applying these equations to ordered intermetallic compounds is that there are many different defects (vacancies and interstitials in either sublattice, and anti-site defects), so separate equations should be written for each. This introduces many new parameters (defect migration and formation energies, recombination reaction volumes, etc.) which have to be supplied for the system of equations to be solved.

A further complication is the interaction between topological and chemical disorder, as exemplified by reactions of the type:

$$A^i \rightarrow B^i + A^B \qquad (17)$$

where an interstitial on an A-site (A^i) decomposes to an interstitial on a B-site (B^i) plus an anti-site defect A^B. This reaction can be energetically favorable [167], and hence chemical disorder can be created by the migration and conversion of interstitials. This means that the recombination term is not the only coupling between the defect balance equations. Also, the migration of these defects is very anisotropic, and is dependent on the concentration of the other defects. It is thus a formidable task to accurately solve the rate equations for defect concentrations in intermetallic compounds. It is however essential to do so in order to predict damage accumulation during irradiation.

If this effort is to succeed, however, it is necessary to obtain reliable values of the defect properties in order that amorphization can be modeled appropriately. Recently the use of new experimental techniques to study the local environment of defects in intermetallic compounds, such as perturbed angular correlation spectroscopy (PACS) [168], Mössbauer, and positron annihilation spectroscopy (PALS) has generated significant data on defect properties of intermetallic compounds. During the past decade, a small but growing number of defect characterization studies have been performed in intermetallic compounds [169]. Collins [170] has used ^{111}In PAC spectroscopy to identify and characterize a variety of thermal and constitutional point defects in B2 ordered compounds such as NiAl, FeAl and CoAl. They used equilibrium thermodynamics to determine binding energies and entropies associated with various defects, which can be used in some cases to

determine actual defect concentrations [171]. Sun and Lin [172] performed positron annihilation lifetime measurements on Ni_3Al. By correlating these results with previous embedded-atom simulations of the Ni_3Al structure [173], they calculated the concentrations of vacancy and antisite defect concentrations as a function of temperature. They found their positron lifetime results to be in good agreement with those of previous researchers [174]. Mössbauer spectroscopy has also been used extensively to study diffusion in intermetallic compounds, [175], such as FeAl [176] and Fe_xTe [177]. The limitations of this technique have been discussed by Petry and Vogl [178]. The results of Hahn and co-workers [179] in PdIn, using ^{119}Sn and ^{57}Fe probes suggest that the two probes can give information about each of the two sublattices. In this case, they were able to study constitutional defects, but their high concentration impeded them from detecting the thermal defects from quenching.

3.3. Transformation mechanisms

Little is known about how the crystalline to amorphous transformation under irradiation actually takes place atomistically (i.e., which specific atomic rearrangements take place). There has been discussion on whether the transformation is first-order or second-order, whether it occurs by nucleation and growth [180], by a gradual rearrangement of atoms that smoothly passes into another phase without discontinuity [181] or finally whether the transformation occurs by a lattice [182] or shear instability [183]. Other studies have detected the presence of precursors to amorphization [154,184], or alternative phase formation paths depending on irradiation conditions [185].

The usual thermodynamic descriptions of first-order and second-order phase transitions in terms of discontinuity of the first or second derivatives of the Gibbs free energy are less useful under irradiation. Since the Gibbs free energy is not a good measure of phase stability under irradiation as mentioned in Section 3.1. Hence, and of necessity, any discussion on the order of phase transitions under irradiation is formally incorrect. However, common usage associates some of the characteristics of first-order and second-order phase transitions with the characteristics of amorphization under irradiation. For example, the coexistence of two phases during phase transition is often cited as evidence of a first order phase transition. Again, the different conditions prevalent under irradiation make such analogies less valid: for example in the case of amorphization by direct cascade impact there is coexistence of phases, but only as a consequence of damage localization. The most relevant question is whether the transformation is continuous and gradual or discontinuous. As argued below, there is actually a continuum between gradual ('2nd-order-like') or discontinuous ('1st-order-like') amorphization phase transitions.

Taking electron irradiation as the simplest type of irradiation to model, since its damage is homogeneous at the atomic level, amorphization can result from a lattice instability due to a large defect concentration, or it can result from a gradual approach to the amorphous state by an accumulation of small local atomic rotations and displacements, within regions smaller than a unit cell. As irradiation continues, more and more of these rotations occur and it becomes progressively easier to effect further rotations. This causes an acceleration of the loss of long-range topological order, or conversely, a shrinkage of the correlation distance between atoms, until only the first and second nearest neighbors are correlated; at that point the sample is amorphous. This most likely occurs when a percolation condition is achieved that renders the remanent crystalline material unstable with respect to the amorphous phase. The computer simulations of Massobrio and Pontikis [186], in Zr_2Ni showed that amorphization occurs when the long-range order parameter S decreased to 0.6. At that level of disorder, amorphization occurs by a percolation of disordered zones through the material.

The other route is for damage to progressively accumulate until at a critical level, there is an elastic or shear instability which causes the lattice to lose most of its crystallinity relatively quickly. Koike [182] proposed a model where amorphization occurs by an elastic instability, after enough defects have accumulated in the lattice. It is difficult to distinguish between those two models as the acceleration of the transformation caused by the cooperative nature of the process is similar to an instability. It should also be noted that molecular dynamics simulations of amorphization do not directly answer the question of whether the transformation is continuous or discontinuous, since transitions that appear gradual in their time scale appear discontinuous in the laboratory. For the case of irradiation, the localization of damage due to displacement cascades is an additional factor.

There is little evidence of a nucleation and growth process taking place during amorphization; the fact that amorphization is easier at low temperature is an indication this mechanism is not dominant. As mentioned above, since long-range diffusion is not needed, amorphization is effected with only local atomic rearrangements. the question is then is amorphization continuous or discontinuous? If as damage accumulates in the lattice it becomes progressively easier to create defects and disorder, the transformation rate always accelerates as amorphization proceeds. It is thus only a question of degree of how cooperative this process is. If there is a great deal of acceleration of the amorphization rate as damage progresses, amorphization would appear as discontinuous, and if not, amorphization would be seen as gradual in the observation time.

The amorphous phase in intermetallic compounds has a lower density than the crystalline phase, a larger dispersion in the nearest neighbor distance and no shear modulus, so it is not surprising that according to any of the formalisms above for calculating the critical damage level, the more

defected a particular region in a crystal, the more favorable it is for amorphization to occur preferentially there. Thus, amorphization is easier near extended defects, as mentioned in Section 2.7. In the same way, the localization of damage creates regions of very high local damage density, so that amorphization occurs first in those regions. As mentioned in Section 2.4, the presence of cascades by causing direct amorphization in cascades or amorphization by cascade overlap extends the amorphization region under ion irradiation compared to electron irradiation. A high dose rate (which can be seen as a localization of the dose in time) also facilitates amorphization.

3.4. Model for amorphization of intermetallic compounds under irradiation

None of the models above answer the fundamental question: *why is the amorphous phase stable under irradiation once it is formed*? To answer this question it is necessary to consider that irradiation causes the material to evolve differently than it would under purely thermal conditions, as the atoms are subjected to random ballistic motions in addition to thermal motions. Under purely thermal conditions the crystalline intermetallic phase is the most stable phase because it implies the greatest degree of both short and long-range order. Under irradiation because of kinetic constraints, that lowest free energy state may not be achievable, and as shown in Fig. 1, the greatest gain of energy comes with the establishment of short-range order, the contribution of long-range order being comparatively smaller. There is evidence that there is a high degree of short-range order (SRO) present in the amorphous phase. The local atomic environment in the amorphous state is very similar to that in the crystalline solid: for example, in the Fe–Zr system a molecular dynamics study showed that the bond lengths, coordination numbers and bond angles in the amorphous material are almost equal to those in the crystalline intermetallic compound Zr_2Fe [187].

As the material accumulates damage, it becomes progressively more difficult to maintain long-range chemical and topological order. At a critical level, the long-range order has degraded enough that it becomes an impediment to maintaining short-range order. That is, if the atoms are not constrained to maintain particular long-range orientation relationships, they can rotate and rearrange themselves locally to maximize the number of nearest neighbor unlike bonds, or to increase the amount of short-range order. This leads to a collective rearrangement of atoms to create a structure where the short-range order is preserved but the long-range order is destroyed. The atomic rearrangements needed to render the material amorphous are only local (smaller than a unit cell), which explains why amorphization can easily occur at lower temperatures. It is interesting to note that atomically-mixed alloys with a *positive* heat of mixing would not necessarily be precluded from amorphization in this mechanism. All this mechanism requires is that there be a constraint on the types of nearest neighbors the atoms are more likely to have (like or unlike atoms). It is only when the atoms are indifferent to how they are arranged that there can be no driving force for amorphization in this mechanism.

Other researchers have proposed similar concepts previously. Turnbull [188] notes that configurationally frozen metastable structures (which amorphous metallic alloys are a part of) can only occur when the kinetically preferred course differs from the thermodynamically preferred one. The material processing route (normally different thermomechanical treatments, here irradiation) opens up new pathways of phase space exploration. He also notes that the kinetically preferred paths tend to be those requiring the least amount of coordination, or the paths of minimum entropy change. Nastasi and Mayer [3] also note that a high degree of steric constraints leads to greater amorphization susceptibility and Johnson [116] notes the fundamental role of kinetics in the amorphization of metallic alloys. It should be mentioned that the formation of metastable phases under irradiation is fundamentally different from normal metallurgical techniques of metastable structure preparation, as the localization of the damage and the irreversible nature of the process create a much different background for microstructural evolution than purely thermal conditions do.

Once formed, the amorphous structure is stable under further irradiation. This means that the atomic displacements caused by irradiation do not cause further changes to the material. The likely reason is that given a random atomic displacement, the high number of atomic arrangements corresponding to the amorphous state causes the atoms to have a high probability of re-forming a local structure with high short-range order once the struck atoms come to rest. Relaxing the constraint of long-range order increases the number of ways that the crystal can arrange itself while maintaining short-range order. Thus, for a given degree of short-range order there are many more micro-states corresponding to a macroscopic amorphous state than there are micro-states corresponding to a damaged crystalline state. The quantity that measures this increase is the entropy, therefore the configurational entropy of the amorphous phase is much higher than that of the irradiated crystalline phase.

Fig. 13 illustrates schematically this entropy-driven amorphization process: defects accumulate in the lattice which raises the enthalpy of the irradiated crystal, ΔH_{irr}. There is a (small) associated entropy increase as more defects increase the configurational entropy, ΔS_{irr}. Assuming that all isenthalpic states are equally probable, when the enthalpy change ΔH_{irr} is equal to ΔH_{ca}, then all the amorphous configurations become equally accessible to the material as the irradiated crystalline structure. The probability of finding the system in any given macrostate is proportional to the number of equivalent microstates or by the entropy of the macrostate. The overall entropy

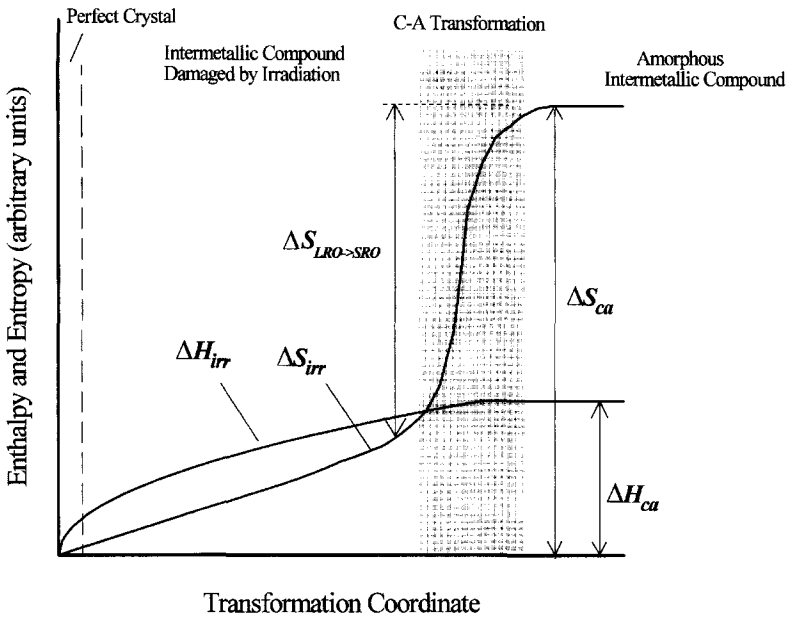

Fig. 13. Schematic representation of the amorphization process. As amorphization proceeds along the transformation coordinate, the enthalpy and entropy of the irradiated crystal increase. As the constraint of long range order is relaxed, the number of configurations with the same degree of short range order abruptly increase compared to the number available in the irradiated crystalline state. From that moment on the system samples exclusively the amorphous structure. Because of the large number of configurations available, the amorphous structure is able to re-form itself after particle impact more easily than a crystalline structure can.

increase from the perfect crystal to the amorphous phase is ΔS_{ca}; the largest fraction of that increase corresponds to $\Delta S_{LRO->SRO}$. The increase in entropy of the damaged crystalline state to the amorphous state $\Delta S_{LRO->SRO}$ corresponds to the increase in the number of ways that the atoms can arrange themselves with a certain degree of short-range order, if they are allowed to relax the constraint of long-range order. If all states of equal enthalpy are equally accessible to the system, the system will find itself most often in the macrostates of greatest entropy, i.e., the amorphous state. The crystal to amorphous transformation occurs within the gray band in Fig. 13, as the entropy suddenly increases. This sudden increase in ΔS_{irr} results from the availability of a large number of amorphous states that are isenthalpic with the damaged crystal. As the system randomly explores all accessible microstates, it finds itself more frequently in the amorphous state.

The question of whether all the iso-energy microstates are equally accessible (i.e. whether the system is ergodic) is difficult to answer. It should be noted here that the exploration of phase space is notably different under irradiation than under thermal conditions [149]. The system is subjected to external forcing in the form of ballistic jumps that are inherently different from the forcing induced by thermal jumps. In particular the ballistic forcing is effective at any temperature, so that the entropy term can be important even at low temperature, differently from the purely thermal case. Thus, although it is reasonable to assume that the regions of phase space explored by the system under irradiation will be different than those explored outside irradiation it is difficult to predict the actual direction of this exploration.

4. Conclusions

The amorphization of intermetallic compounds by irradiation is an interesting and fruitful research field, with impact on many other related fields. Irradiation-induced amorphization is a complex phenomenon, affected by various irradiation parameters and dependent on the irradiating particle, temperature and material properties. Progress has been made on understanding the transformation mechanisms and associated driving forces, but there is still great potential for future work. Promising areas of research include the use of amorphization to study the properties of intermetallic compounds, and the combined use of computer simulation, irradiations, and nuclear probe techniques to better understand and quantitatively describe the amorphization process. A few important points are emphasized from the foregoing discussion:

(1) Amorphization is easier at low temperatures, due to the absence of dynamic annealing. As the irradiation temperature is increased, different annealing stages corresponding to the activation energies of different defects are reached. These annealing stages make amorphization progressively more difficult until at the critical temperature

T_c, the annealing rate is larger than the damage rate and amorphization is no longer possible.

(2) The severity of the damage (damage localization in time or in space) has great influence on amorphization. Both higher dose rates and denser displacement cascades, corresponding to damage localization in space and in time, make amorphization easier. The critical temperature for cascade-producing irradiation is higher than for electron irradiation, and the critical temperature for ion and electron irradiation is higher for higher dose rates.

(3) The presence of extended defects (dislocations, stacking faults), and departures from the ideal compound stoichiometry also facilitate amorphization. The influence of sample orientation and electron energy has also been studied, and related to the different displacement energies in different crystalline orientations and in the individual sublattices.

(4) Amorphization occurs after a critical irradiation dose has been delivered to the material. Several models exist to calculate that critical damage level. The amorphization process is controlled by the accumulation of damage in the material, so a predictive model of amorphization has to include the modeling of irradiation kinetics.

(5) Amorphization does not depend on long-range defect diffusion, since it occurs more readily at low temperature. Therefore the transformation takes place by a cooperative process, involving only local atomic rearrangements, and unit cell rotations. This is made possible by relaxing the constraints of long-range order so that short-range order can be maintained.

(6) Once made amorphous, an intermetallic compound is stable under further irradiation. This stability is likely caused by a greater availability of microstates corresponding to an amorphous structure than to a crystalline structure when the material explores phase space under external forcing by irradiation.

Acknowledgements

The author is greatly indebted to all his collaborators and colleagues for helping develop these ideas about amorphization. Fruitful and stimulating discussions with L.M. Howe, P.R. Okamoto, N.Q. Lam, D.R. Olander, C. Lemaignan, P. Desré and G. Martin are specially acknowledged. R.C. Birtcher and W.J. Weber provided useful comments on the manuscript.

References

[1] R.C. Ewing, Nucl. Instr. Meth. Phys. Res. B 91 (1994) 22–29; L.M. Wang and R.C. Ewing, Mater. Res. Soc. Bull. 5 (1992) 38–44.
[2] M.L. Swanson, J.R. Parsons and C.W. Hoelke, Rad. Eff. 9 (1971) 249–256.
[3] M. Nastasi and J.W. Mayer, Mater. Sci. Rep. 6 (1991) 1.
[4] P.R. Okamoto and M. Meshii, in: Science of Advanced Materials, eds. H. Wiedersich and M. Meshii (ASM, 1992) pp. 33–98.
[5] D.E. Luzzi and M. Meshii, Res. Mech. 21 (1987) 207–247.
[6] C. Jaouen, Solid State Phen. 23–24 (1992) 123–146.
[7] A.T. Motta and C. Lemaignan, in: Ordering and Disordering in Alloys, ed. A.R. Yavari (Elsevier, 1992) pp. 255–276.
[8] D.F. Pedraza, Metall. Trans. 21A (1990) 1809–1815.
[9] W.L. Johnson, Prog. Mater. Sci. 30 (1986) 81–134.
[10] N.Q. Lam and P.R. Okamoto, Mater. Res. Soc. Bull. May (1994) 41–46.
[11] A.D. Korotaev and A.N. Tyumentsev, Russ. Phys. J. 37(8) (1994) 703–724.
[12] H. Mori, H. Fujita, M. Tendo and M. Fujita, Scr. Metall. 18 (1984) 783–88.
[13] L.J. Gallego, J.A. Somoza, H.M. Fernandez and J.A. Alonso, in: Ordering and Disordering in Alloys, ed. A.R. Yavari (Elsevier, 1992) pp. 328–335.
[14] J.L. Brimhall, H.E. Kissinger and A.R. Pelton, Rad. Eff. 70 (1985) 241–258.
[15] D.E. Luzzi and M. Meshii, Scr. Metall. 20 (1986) 943–948.
[16] D.T. Kulp, T. Egami, D.E. Luzzi and V. Vitek, J. Alloys Compounds 194 (1993) 417–427.
[17] N. Karpe, Nucl. Instrum. Methods Phys. Res. B 95 (1995) 4850–490.
[18] C. Jaouen, J. Delafond and J.P. Rivière, J. Phys. F 17 (1987) 335.
[19] R.J. Gaboriaud, J.J. Grob and F. Abel, Nucl. Instrum. Methods Phys. Res. B 19–20 (1987) 648–653.
[20] A. Mehrtens, G. von Minnigerode, D. Oegelschlager and K. Samwer, Z. Physik B 88 (1992) 25–34.
[21] A. Paesano, S.R. Teixeira and L. Amaral, Hyperfine Interact. 67 (1991) 665–670.
[22] N. Cowlam, Key Eng. Mater. 103 (1995) 125–162.
[23] K.N. Kushita, K. Hojou and S. Furuno, J. Electron Microsc. 44 (1995) 456–461.
[24] J. Cheng, M. Yuan, C.N.J. Wagner and A.J. Ardell, J. Mater. Res. 4(3) (1989) 565–578.
[25] E.G. Ponyatovsky and O.I. Barkalov, Mater. Sci. Rep. 8(4) (1991) 147–191.
[26] L.-M. Wang and R.C. Ewing, Mater. Res. Soc. Bull. 17 (5) (1992) 38–44.
[27] H. Inui, H. Mori and H. Fujita, Acta Metall. 37(5) (1989) 1337–1342.
[28] H.M. Naguib and R. Kelly, Rad. Eff. 25 (1975) 1–12.
[29] R.C. Ewing and L.-M. Wang, Nucl. Instrum. Methods Phys. Res. B 65 (1992) 319–323.
[30] W.J. Weber, J. Am. Ceram. Soc. 76(7) (1993) 1729–1738.
[31] W.J. Weber, R.C. Ewing and L.-M. Wang, J. Mater. Res. 9(3) (1994) 688–698.
[32] H. Inui, H. Mori and H. Fujita, Philos. Mag. B 61(1) (1990) 107–124.
[33] F.W. Clinard and L.W. Hobbs, Radiation Effects in Non-Metals, in: Physics of Radiation Effects in Crystals, eds. R.A. Johnson and A.N. Orlov (Elsevier, 1986) pp. 387–471.
[34] L.-M. Wang, W.L. Gong, R.C. Ewing and W.J. Weber, Mater. Res. Soc. Fall 1995 Symp. Proc. Vol. 398, eds. J.S. Im, G.B. Stephenson, A.L. Greer and B. Park, pp. 233–238.
[35] C. Kinoshita, Y. Isobe, H. Abe, Y. Denda and T. Sonoda, J. Nucl. Mater. 206 (1993) 341–352.
[36] H. Abe, H. Naramoto and C. Kinoshita, Mater. Res. Soc.

Symp. Proc. Vol. 373, eds. I.M. Robertson, L.E. Rehn, S.J. Zinkle and W.J. Phythian (1995) pp. 383–388.
[37] S.J. Zinkle and L.L. Snead, Nucl. Instrum. Methods Phys. Res. B 116 (1996) 92–101.
[38] N. Yu, K.E. Sickafus and M. Nastasi, Mater. Res. Soc. Symp. Proc. 373 (1995) 401–406.
[39] R. Devanathan, N. Yu, K.E. Sickafus, M. Nastasi and Mater. Res. Soc. Symp. Proc. 398 (1996) 171–177.
[40] L.W. Hobbs, J. Non-Cryst. Solids 182 (1995) 27–39.
[41] S.M. Sharma and S.K. Sikka, Prog. Mater. Sci. 40 (1996) 1–77.
[42] L. Douillard and J.P. Duraud, Nucl. Instrum. Methods Phys. Res. B 107 (1996) 212–217.
[43] R.B. Winters and W.S. Hammack, Science 260 (1993) 202–204.
[44] W.J. Weber and L.M. Wang, Nucl. Instrum. Methods Phys. Res. B 106 (1995) 298–302.
[45] H. Inui, H. Mori and T. Sakata, Philos. Mag. B 61 (1990) 107; 66 (1992) 737.
[46] W.J. Weber, L.-M. Wang, N. Yu and N.J. Hess, Mater. Res. Soc. Fall 1995 Symp. Proc. Vol. 398, eds. J.S. Im, G.B. Stephenson, A.L. Greer and B. Park, pp. 351–356.
[47] L.C. Qin and L.W. Hobbs, Mater. Res. Soc. Symp. Proc. 284 (1993) 331.
[48] V. Radmilovic, R. Kilaas and G. Thomas, Proc. 52nd Ann. Meeting of the Microsc. Soc. of Am. eds. G.W. Bailey and A.J. Garrat-Reed (San Francisco Press, San Francisco, 1994) pp. 662–663.
[49] D.E. Luzzi and M. Meshii, J. Mater. Res. 1(5) (1986) 617–628.
[50] A. Serebryakov, Scr. Metall. Mater. 28 (1993) 1011–1016.
[51] L.W. Hobbs, Nucl. Instrum. Methods Phys. Res. B 91 (1994) 30–42.
[52] A. Battaglia, J. Appl. Phys. 74(10) (1993) 6058.
[53] T. Bachmann, R. Schulz, E. Glaser, U. Richter and S. Schippel, Nucl. Instrum. Methods Phys. Res. B 106 (1995) 350–354.
[54] R.D. Goldberg, J.S. Williams and R.G. Elliman, Nucl. Instrum. Methods Phys. Res. B 106 (1995) 242–247.
[55] G. Carter, J. Appl. Phys. 79(11) (1996) 8285–8289.
[56] H. Abe, C. Kinoshita, P.R. Okamoto and L.E. Rehn, J. Nucl. Mater. 212–215 (1994) 298–302.
[57] H. Abe, C. Kinoshita, Y. Isobe, Y. Denda and T. Sonoda, Proc. Jpn. Acad. B 69(7) (1993) 173–178.
[58] D.N. Seidman, R.S. Averback, P.R. Okamoto and A.C. Bailey, Mater. Res. Soc. Symp. Proc. eds. H. Kurtz, G.L. Olson, J.M. Poate (1987) pp. 349–355.
[59] G. Compagnini and L. Calcagno, Mater. Sci. Eng. R 13(5,6) (1994) 193–263.
[60] K. Niwase, Phys. Rev. B 52(22) (1995) 15785–15798.
[61] K. Niwase, K. Nakamura, T. Shikama and T. Tanabe, J. Nucl. Mater. 170 (1990) 106–108.
[62] S.J. Pennycook, R. Feenstra, M.F. Chisholm and D.P. Norton, Nucl. Instrum. Methods Phys. Res. B 79 (1993) 641–644.
[63] S.N. Basu, T.E. Mitchell and M. Nastasi, J. Appl. Phys. 69(5) (1991) 3167–3171.
[64] C.C. Koch, O.B. Cavin, C.G. McKamey and J.O. Scarbrough, Appl. Phys. Lett. 43 (1983) 1017.
[65] H. Bakker, G.F. Zhou and H. Yang, Prog. Mater. Sci. 39 (1995) 159–241.
[66] U. Herr, Key Eng. Mater. 103 (1995) 113–124.
[67] V.A. Pavlov, J. Mater. Sci. 28 (1993) 5443–5450.
[68] J. Meng, P.R. Okamoto, L.J. Thompson, B.J. Kestel and L.E. Rehn, Appl. Phys. Lett. 53 (1988) 1820–1822.
[69] K. Aoki and T. Matsumoto, J. Alloys Compounds 194 (1993) 251–261.
[70] K. Aoki and T. Matsumoto, J. Alloys Compounds 231 (1995) 20–28.
[71] A. Audouard, E. Balanzat, S. Bouffard, J.C. Jousset, A. Chamberod, A. Dunlop, D. Lesueur, G. Fuchs, R. Spohr, J. Vetter and L. Thome, Phys. Rev. Lett. 65(7) (1990) 875–878.
[72] D.K. Tappin, I.M. Robertson and H.K. Birnbaum, Phys. Rev. B 51(21) (1995) 14854–14860.
[73] J. Jagielski and M. Kopcewicz, J. Appl. Phys. 73(10) (1993) 4820–4824.
[74] C. Rodriguez, R.H. de Tendler, L.J. Gallego and J.A. Alonso, J. Mater. Sci. 30 (1995) 196–200.
[75] E. Ma and M. Atzmon, Mater. Chem. Phys. 39 (1995) 249–267.
[76] A. Crespo-Sosa, P. Schaaf, W. Bolse, K.-P. Lieb, M. Gimbel, U. Geyer and C. Tosello, Phys. Rev. B 53(22) (1996) 14795–14805.
[77] U. Gösele an K.N. Tu, J. Appl. Phys. 66(6) (1989) 2619–2626.
[78] A. Paesano and A.T. Motta, R.C. Birtcher, E.A. Ryan, L. Amaral, M. Bruckmann and S.R. Teixeira, Mater. Res. Soc. Fall Proc. (1996) accepted.
[79] M. Nastasi and J.W. Mayer, Mater. Sci. Eng. R 12 (1994) 1–52.
[80] F.R. Ding, P.R. Okamoto and L.E. Rehn, Nucl. Instrum. Methods Phys. Res. B 39 (1989) 122.
[81] J. Koike, P.R. Okamoto, L.E. Rehn and M. Meshii, J. Mater. Res. 4(5) (1989) 1143–1150.
[82] A.T. Motta, F. Lefebvre and C. Lemaignan, ASTM STP 1132 (1991) 718–739.
[83] G.J.C. Carpenter and E.M.Schulson, J. Nucl. Mater. 23 (1978) 180.
[84] E.M. Schulson, G.J.C. Carpenter and L.M. Howe, J. Nucl. Mater. 82 (1979) 140.
[85] L.M. Howe and M. Rainville, J. Nucl. Mater. 68 (1977) 215–234.
[86] L.M. Howe and M. Rainville, Phil. Mag. A 39(2) (1979) 195–212.
[87] P. Bellon and G. Martin, in: Ordering and Disordering in Alloys, ed. A.R. Yavari (Elsevier, 1992) pp. 172–181.
[88] L.E. Rehn and R.C. Birtcher, J. Nucl. Mater. 205 (1993) 31–39.
[89] A.T. Motta, D.R. Olander and A.J. Machiels, ASTM STP 1046 (1989) eds. N.H. Packan, R.E. Stoller and A.S. Kumar, pp. 457–469.
[90] L.M. Howe, D. Philips, A.T. Motta and P.R. Okamoto, Surf. Coatings Technol. 66 (1994) 411–418.
[91] A.T. Motta, L.M. Howe and P.R. Okamoto, J. Nucl. Mater. 205 (1993) 258–266.
[92] D.F. Pedraza and L.K. Mansur, Nucl. Instrum. Methods Phys. Res. B 16 (1986) 203–211.
[93] G.B. Xu, Ph.D. thesis, Northwestern University (1994).
[94] A.T. Motta, L.M. Howe and P.R. Okamoto, unpublished research.
[95] L.M. Howe, M.H. Rainville and D. Philips, Mater. Res.

Soc. Symp. Proc. 235, eds. G.S. Was, L.E. Rehn and D.M. Follstaedt (1992) p. 461.
[96] M. Griffiths, R.W. Gilbert and G.J.C. Carpenter, J. Nucl. Mater. 150 (1987) 53–66.
[97] A.T. Motta and C. Lemaignan, J. Nucl. Mater. 195 (1992) 277–285.
[98] J. Koike, P.R. Okamoto, L.E. Rehn and M. Meshii, Mater. Res. Soc. Symp. Proc. 157, eds. J.A. Knapp, P.B. Borgessen and R.A. Bahr (1990) p. 777.
[99] J.L. Brimhall, H.E. Kissinger and L.A. Charlot, Rad. Eff. 77 (1983) 237–293.
[100] D.M. Parkin and R.O. Elliott, J. Mater. Res. 3(3) (1988) 453–460.
[101] L.M. Howe, D.P. McCooeye, M.H. Rainville, J.D. Bonnett and D. Phillips, Nucl. Instrum. Methods Phys. Res. B 59 (1991) 884.
[102] A.J. Ardell and K. Janghorban, J. Non-Cryst. Solids 65 (1984) 73–86.
[103] P.M. Ossi, Phys. Stat Sol. (a) 119 (1990) 463–470.
[104] D.L. Beke, H. Bakker and P.I. Loeff, Coll. Phys. C 4, Suppl. 14, tomme 51 (1990) 63–69.
[105] M. Nastasi, J.M. Williams, E.A. Kenik and J.W. Mayer, Nucl. Instrum. Methods Phys. Res. B 19/20 (1987) 543–548.
[106] P. Moine and C. Jaouen, J. Alloys Compounds, 194 (1993) 373–380.
[107] J.F. Gibbons, Proc. IEEE 60 (1972) 1062.
[108] D.F. Pedraza, Phys. Rev. B 38(7) (1988) 4803–4809.
[109] J. Koike, P.R. Okamoto, L.E. Rehn and M. Meshii, Metall. Trans. A 21 (1990) 1799–1808.
[110] A. Mogro-Campero, E.L. Hall, J.L. Walter and A.J. Ratkowski, in Metastable Phase Formation by Ion Implantation, eds. S.T. Picraux, W.J. Choike (Elsevier, Lausanne, 1982) pp. 203–210.
[111] G. Thomas, H. Mori, H. Fujita and R. Sinclair, Scr. Metall. 16 (1982) 589–592.
[112] H. Mori, M. Nakajima and H. Fujita, Proc. XIth Int. Cong. on Electron Microsc. Kyoto (1986) pp. 1101–1102.
[113] H. Mori, H. Fujita and M. Fujita, Jpn. J. Appl. Phys. 22(2) (1983) L94–L96.
[114] D.E. Luzzi, H. Mori, H. Fujita and M. Meshii, Acta Metall. 34(4) (1986) 629–639.
[115] D.E. Luzzi, H. Mori, H. Fujita and M. Meshii, Mater. Res. Soc. Symp. Proc. Vol. 51, eds. H. Kurz, G.L. Olson and J.M. Poate (1986) pp. 479–484.
[116] W.L. Johnson, Mat. Sci. Eng. 97 (1988) 1–13.
[117] R. Devanathan, N.Q. Lam, P.R. Okamoto and M. Meshii, Mater. Res. Soc. Symp. Proc. Vol. 291 Fall 1992, eds. P.D. Bristowe, J. Broughton and J.M. Newsam.
[118] D.T. Kulp, T. Egami, D.E. Luzzi and V. Vitek, Mater. Res. Soc. Symp. Proc. Vol. 279 Fall 1992, eds. M.A. Nastasi, N. Herbots, L.R. Harriott and R.S. Averback.
[119] P.R. Okamoto, L.E. Rehn, J. Pearson, R. Bhadra and M. Grimsditch, J. Less-Common Metals 140 (1988) 231–244.
[120] R. Devanathan, N.Q. Lam, P.R. Okamoto and M. Meshii, Mater. Res. Soc. Symp. Proc. Vol. 279 Fall 1992, eds. M.A. Nastasi, N. Herbots, L.R. Harriott and R.S. Averback.
[121] D. Wolf, P.R. Okamoto, S. Yip, J.F. Lustko and M. Kluge, J. Mater. Res. 5(2) (1990) 286–300.
[122] J. Bloch, J. Nucl. Mater. 6 (1962) 203.
[123] A.V. Mirmelshtein, A.Y. Karkin, V.Y. Arkhipov and V.I. Voronin, Phys. Met. Metall. 55 (1983) 67.
[124] A.R. Sweedler, D.E. Cox and S. Moehlecke, J. Nucl. Mater. 72 (1978) 50–69.
[125] S.M. Cheremisin, A.Yu. Dudkin and I.V. Matveev, Nucl. Instrum. Methods Phys. Res. B 84 (1994) 102–104.
[126] L.L. Harris and W.J.S. Yang, 13th Int. Symp. on the Effects of Irradiation on Materials, eds. F.A. Garner, N.H. Packan and A.S. Kumar, ASTM STP 955 (1987) 661.
[127] W.J.S. Yang, personal communication.
[128] K. Farrell, Mater. Res. Soc. Symp. Proc. 373 (1995) 165–170.
[129] R.W. Gilbert, M. Griffiths and G.J.C. Carpenter, J. Nucl. Mater. 135 (1985) 265–268.
[130] W.J.S. Yang, R.P. Tucker, B. Cheng and R.B. Adamson, J. Nucl. Mater. 138 (1986) 185–195.
[131] A.T. Motta, L.M. Howe and P.R. Okamoto, Mater. Res. Soc. Symp. Proc. Vol. 279 Fall 1992, eds. M.A. Nastasi, N. Herbots, L.R. Harriott and R.S. Averback.
[132] R. Kruger and R.B. Adamson, J. Nucl. Mater. 205 (1993) 242–250.
[133] R.C. Birtcher, J.W. Richardson, Jr. and M.H. Mueller, Mater. Res. Soc. Symp. Proc. Vol. 373, eds. I.M. Robertson, L.E. Rehn, S.J. Zinkle and W.J. Phythian (1995) pp. 227–232.
[134] R.C. Birtcher, L.E. Rehn and G.L. Hoffman, J. Nucl. Mater. 152 (1988) 73.
[135] J. Koike, D.E. Luzzi, M. Meshii and P.R. Okamoto, Mater. Res. Soc. Symp. Proc. 74 (1987) 425–530.
[136] J. Faldowski, A.T. Motta, L.M. Howe and P.R. Okamoto, Mater. Res. Soc. Fall 1995 Symp. Proc. Vol. 398, eds. J.S. Im, G.B. Stephenson, A.L. Greer and B. Park, pp. 183–188.
[137] E. Goo, A. Murthy and C.J.D. Hetherington, Scr. Metall. Mater. 29 (1993) 553–555.
[138] A.T. Motta, L.M. Howe and P.R. Okamoto, Mater. Res. Soc. Symp. Proc. Vol. 316, eds. R.J. Culbertson, O.W. Holland and K. Maex (1994) pp. 265–271.
[139] D. Pecheur, A.T. Motta and C. Lemaignan, J. Nucl. Mater. 195 (1992) 221–227.
[140] J.A. Faldowski, A.T. Motta, L.M. Howe and P.R. Okamoto, J. Appl. Phys. 80(2) (1996) 729–733.
[141] L.M. Howe, Nucl. Instrum. Methods Phys. Res. B, to be published.
[142] A. Matsunaga, C. Kinoshita, K. Nakai and Y. Tomokiyo, J. Nucl. Mater. 179–181 (1991) 457–460.
[143] T. Egami and Y. Waseda, J. Non-Cryst. Solids 64 (1984) 113–1334.
[144] J. Bletry, Philos. Mag. B 62(5) (1990) 469–508.
[145] P. Bellon, F. Soisson, G. Martin and F. Haider, Solid State Phen. 23–24 (1992) 169–180.
[146] G. Martin, Phys. Rev. B 21(6) (1980) 2122–2130.
[147] K.C. Russell, Prog. Mater. Sci. 28 (1985) 229.
[148] G. Martin, Phys. Rev. B 30(3) (1984) 1424–1436.
[149] P. Bellon and G. Martin, Mater. Res. Soc. Bull. 11(12) (1991) 33–36.
[150] K.Y. Liou and P. Wilkes, J. Nucl. Mater. 87 (1979) 317.
[151] P. Gordon, Principles of Phase Diagrams (McGraw-Hill, 1968).
[152] A.T. Motta and D.R. Olander, Acta Metall. Mater. 38(11) (1990) 2175–2185.

[153] E.P. Simonen, Nucl. Instrum. Methods Phys. Res. B 16 (1986) 198–202.
[154] D.E. Luzzi, J. Mater. Res. 6(10) (1991) 2059–2068.
[155] A.D. Brailsford and R. Bullough, J. Nucl. Mater. 44 (1972) 121–135; L.K. Mansur, Nucl. Technol. 40 (1978) 5–34.
[156] S. Banerjee and K. Urban, Phys. Status Sol. (a) 81 (1984) 145–162.
[157] R. Zee and P. Wilkes, Philos. Mag. A 42 (1980) 463–482.
[158] J. Wang, S. Yip, S. Phillpot and D. Wolf, J. Alloys Compounds 194 (1993) 407–415.
[159] F.A. Lindemann, Z. Physik 11 (1910) 609.
[160] K. Kusunoki, Phys. Rev. B 53(1) (1996) 16–19.
[161] G.B. Xu, M. Meshii, P.R. Okamoto and L.E. Rehn, J. Alloys Compounds 194 (1993) 401–405.
[162] A.T. Motta, L.M. Howe and P.R. Okamoto, Mater. Research Soc. Symp. Proc. Vol. 373, eds. I.M. Robertson, L.E. Rehn, S.J. Zinkle and W.J. Phythian (1995) pp. 183–188.
[163] M. Li, W.L. Johnson and W.A. Goddard, Mater. Sci. Forum 179–181 (1995) 855–866.
[164] H.J. Fecht, Nature 356(12) (1992) 133–135.
[165] A.V. Granato, J. Phys. Chem. Solids 55(10) (1994) 931–939.
[166] A.V. Granato, Phys. Rev. Lett. 68 (1992) 974.
[167] J.R. Shoemaker, R.T. Lutton, D. Wesley, W.R. Wharton, M.L. Oehrli, M.S. Herte, M.J. Sabochik and N.Q. Lam, J. Mater. Res. 6(3) (1991) 473–482.
[168] G.L. Catchen, Mater. Res. Soc. Bull. 20(7) (1995) 37–46.
[169] W. Pfeiffer, M. Deicher, R. Keller, R. Magerle, P. Pross, H. Skudik, Th. Wichert, H. Wolf, D. Forkel, N. Moriya and R. Kalish, Appl. Surf. Sci. 50 (1991) 154–158.
[170] G.S. Collins, Hyperfine Interact. 80(1–4) (1993) 1257–1262.
[171] J. Fan and G.S. Collins, Hyperfine Interact. 79 (1993) 745.
[172] J. Sun and T.L. Lin, Acta Metall. 42(1) (1994) 195–200.
[173] T.L. Lin and D. Chen, J. Phys. Coll. C 1 (1990) 227–232.
[174] A. Dasgupta, L.C. Smedskjaer, D.G. Legnini and R.W. Siegel, Mater. Lett. 3 (1985) 457.
[175] F. Aubertin, U. Gonser, S.J. Campbell and H.G. Wagner, Z. Metallkde. 76 (1985) 237–244.
[176] G. Vogl and B. Sepio, Acta Metall. Mater. 42(9) (1994) 3175–3181.
[177] M. Magara, T. Tsuji and K. Naito, Defect Diff. Forum 95–98 (1993) 887–892.
[178] W. Petry and V. Vogl, Mater. Sci. Forum 15–18 (1987) 323.
[179] H. Hahn, M. Ghafari, R. Dieudonne and U. Gonser, Scr. Metall. 19 (1985) 615–619.
[180] P. Maziasz, N.H. Packan, D.F. Pedraza and J.P. Simmons, J. Mater. Res. 5(5) (1990) 932–941.
[181] N.Q. Lam and P.R. Okamoto, Surf. Coatings Technol. 66 (1994).
[182] J. Koike, Phys. Rev. B 47 (13) (1993) 7700–7704.
[183] J. Koike, P.R. Okamoto, L.E. Rehn and M. Meshii, Nucl. Instrum. Methods Phys. Res. B 59/60 (1991) 471–474.
[184] Ch. Wirtz, A. Blatter, N. Baltzer and M. von Allmen, Phys. Rev. B 42(11) (1990) 6993–6999.
[185] K. Urban, S. Banerjee and J. Mayer, Mater. Sci. Forum (1985) 335–352.
[186] C. Massobrio and V. Pontikis, Phys. Rev. B 45(5) (1992) 2484.
[187] Ch. Hausleitner and J. Hafner, J. Non-Cryst. Solids 144 (1992) 175–186.
[188] D. Turnbull, Metall. Trans. B 12 (1981) 217–230.